THE α-$\mathcal{F}$ COMPOSITE DISTRIBUTION WITH POINTING ERRORS: CHARACTERIZATION, PERFORMANCE AND APPLICATIONS

PEDRO HENRIQUE DORNELAS ALMEIDA

MASTER'S THESIS
IN ELECTRICAL ENGINEERING

DEPARTMENT OF ELECTRICAL ENGINEERING

FACULTY OF TECHNOLOGY

UNIVERSITY OF BRASÍLIA

University of Brasília
Faculty of Technology
Department of Electrical Engineering

The α-$\mathcal{F}$ Composite Distribution with Pointing Errors: Characterization, Performance and Applications

Pedro Henrique Dornelas Almeida

MASTER'S THESIS SUBMITTED TO THE POST-GRADUATE PROGRAM IN ELECTRICAL ENGINEERING OF THE UNIVERSITY OF BRASÍLIA AS PART OF THE REQUIREMENTS NECESSARY TO OBTAIN THE MASTER'S DEGREE.

APPROVED BY:

Hugerles Sales Silva, Dr. (University of Brasília)
(Supervisor)

Ugo Silva Dias, Dr. (University of Brasília)
(Co-supervisor)

Tarcisio Ferreira Maciel, Dr. (Federal University of Ceará)
(External Examiner)

Robson Domingos Vieira, Dr. (University of Brasília)
(Internal Examiner)

Brasília/DF, October/2024.

FICHA CATALOGRÁFICA

ALMEIDA, PEDRO

The α-$\mathcal{F}$ Composite Distribution with Pointing Errors: Characterization, Performance and Applications. [Brasília/DF] 2024.

viii, 51p., 210 x 297 mm (ENE/FT/UnB, Master, Master's Thesis, 2024).

University of Brasilia, Faculty of Technology, Department of Electrical Engineering.

Department of Electrical Engineering

1. α-$\mathcal{F}$ distribution
2. Multihop
3. NOMA
4. Performance metrics
5. Pointing Errors
6. Terahertz Systems

I. ENE/FT/UnB
II. Título (série)

REFERÊNCIA BIBLIOGRÁFICA:

ALMEIDA, PEDRO (2024). The α-$\mathcal{F}$ Composite Distribution with Pointing Errors: Characterization, Performance and Applications. Master's Thesis, Department of Electrical Engineering, Publication PPGEE DM-819/24, University of Brasília, Brasília, DF, 66p.

Pedro Almeida

Universidade de Brasília (UnB)

Campus Darcy Ribeiro

Faculdade de Tecnologia - FT

Departamento de Engenharia Elétrica (ENE)

Brasília - DF, CEP 70919-970

Dedico este trabalho aos meus pais, à minha família, aos amigos e a todos que me apoiaram e ajudaram durante esta jornada. Dedico também aos professores que contribuíram para esta etapa e me incentivaram desde o princípio a seguir a carreira acadêmica.

RESUMO

A distribuição de desvanecimento composta α-$\mathcal{F}$ com erros de apontamento: caracterização, desempenho e aplicações.

A distribuição de desvanecimento composta α-$\mathcal{F}$ com erros de apontamento é proposta neste trabalho. Novas expressões são derivadas para a função densidade de probabilidade e função de distribuição cumulativa do envelope/relação sinal-ruído instantânea (SNR), momentos de ordem superior e função geratriz de momentos da SNR instantânea. Com base nas estatísticas mencionadas acima, expressões são obtidas para a probabilidade de indisponibilidade, probabilidade de erro de símbolo e capacidade ergódica do canal. Análises assintóticas também são fornecidas. Diversos cenários são estudados, como a aplicação do modelo α-$\mathcal{F}$ com erros de apontamento em cenários com múltiplos saltos, superfícies inteligentes reconfiguráveis (RIS) e sistemas de acesso múltiplo não ortogonal (NOMA). Diversas curvas, corroboradas por simulações de Monte Carlo, são apresentadas para diferentes valores que caracterizam os parâmetros do canal. Todas as expressões deduzidas neste trabalho são inéditas.

Palavras-chave: Distribuição α-$\mathcal{F}$, erros de apontamento, múltiplos saltos, NOMA e métricas de desempenho.

ABSTRACT

The α-$\mathcal{F}$ composite fading distribution with pointing errors is proposed in this work. New expressions for the probability density function and cumulative distribution function of the envelope/instantaneous signal-to-noise ratio (SNR), higher-order moments, and moment generation function of the instantaneous SNR are derived. Based on the above-mentioned statistics, expressions for the outage probability, symbol error probability, and ergodic channel capacity are obtained. The asymptotic analyses are also provided. Several scenarios are studied, such as the application of the α-$\mathcal{F}$ model with pointing errors concerning multihop, reconfigurable intelligent surfaces (RIS), and non-orthogonal multiple access (NOMA) systems. Several curves, corroborated by Monte Carlo simulations, are presented for different values that characterize the channel parameters. All expressions deduced in this work are new.

Keywords: α-$\mathcal{F}$ distribution, pointing errors, multihop, NOMA and performance metrics.

CONTENTS

LIST OF FIGURES

LIST OF SYMBOLS

α	Non-linearity of the channel
e	Euler's number
$\exp(\cdot)$	Exponential function
Y	Received signal
X	Transmitted signal
W/w_l	Additive white Gaussian noise
H	Total gain
h_l	Path loss
H_f	Composite fading channel
H_p	Misalignment component
$\mathrm{H}[\cdot]$	Fox-H function
$\mathrm{H}[\cdot\|\cdot\|\cdot]$	Multivariate Fox H-function
c	Speed of light
f	Operating frequency
d	Distance between the transmitter and the receiver
h_{al}	Molecular absorption gain
h_{fl}	Propagation gain
$\kappa(f)$	Absorption coefficient
μ	Number of multipath clusters
$\mathrm{B}(\cdot,\cdot)$	Beta function
m	Shadowing parameter
$\mathcal{M}[\cdot]$	Mellin transform
$\hat{r}$	α-root mean value
$\mathbb{E}(\cdot)$	Expectance operator
z	Pointing error parameter
A_0	Fraction of the collected power
$\Gamma(\cdot)$	Gamma function
γ	Signal-to-noise ratio
$\bar{\gamma}$	Average signal-to-noise ratio
γ_{th}	SNR OP threshold
$\mathrm{M}_\Gamma(\gamma)$	Moment generation function
$f_\Gamma(\gamma)$	Probability density function
$F_\Gamma(\gamma)$	Cumulative distribution function
${}_2\mathrm{F}_1[\cdot,\cdot,\cdot;\cdot]$	Gauss hypergeometric function
$\min(\cdot)$	Minimum operator
$\arg\min(\cdot)$	Argument that the minimum operator finds
θ	Modulation parameter

ρ	Modulation type
$\psi(\cdot)$	Digamma function
C_{erg}	Ergodic capacity
C_{erg}^{∞}	Asymptotic ergodic capacity
P_{out}	Outage probability
P_{out}^{∞}	Asymptotic outage probability
P_{sym}	Symbol error probability
P_{sym}^{∞}	Asymptotic symbol error probability
P_{b}	Bit error probability
P_{b}^{∞}	Asymptotic bit error probability
u	Time-bandwidth product under the energy detection technique
G_d	Diversity gain
G_r	Gain of the receive antenna
G_t	Gain of the transmit antenna
$G[\cdot]$	Meijer-G function
$Q(\cdot)$	Gaussian Q-function
$\binom{\cdot}{\cdot}$	Binomial coefficient
δ	Distance/difference of symbols (complex numbers)
$\Re\{\cdot\}$	Real part operator
$(\cdot)^*$	Complex conjugate

GLOSSARY

5G	Fifth-generation
5G+	Fifth generation and beyond
AUC	Area under the receiver operating characteristics
BEP	Bit error probability
BER	Bit error rate
BPSK	Binary phase-shift keying
BS	Base station
CDF	Cumulative distribution function
FSO	Free space optics
LoS	Line of sight
MGF	Moment generating function
MIMO	Multiple-input multiple-output
MISO	Multiple-input single-output
MLD	Maximum likelihood detection
MSE	Mean square error
NOMA	Non-orthogonal multiple access
PDF	Probability density function
PEP	Pairwise error probability
QPSK	Quadrature phase-shift keying
RF	Radio frequency
RIS	Reconfigurable intelligent surface
RV	Random variable
SEP	Symbol error probability
SIC	Successive interference cancellation
SNR	Instantaneous signal-to-noise ratio
OP	Outage probability
THz	Terahertz

CHAPTER 1

INTRODUCTION

1.1 SCOPE AND MOTIVATION

Nowadays, the fifth generation (5G) of mobile communications is a promising and essential technology to meet the high demands and requirements of new vertical use cases. In order to support it, terahertz (THz) band frequencies have attracted the interest of several researchers around the world, mainly due to the broader available spectrum, higher throughputs, and for supporting a greater number of simultaneous users [1]. As disadvantages, THz bands present high atmospheric attenuation, which can be compensated by the system using high-directional antenna arrays. However, in this scenario, a misalignment between the transmitting and receiving antennas can occur, a phenomenon well-known as pointing error [2]. Vibrations, mechanical noise, position estimation errors, air pressure, and wind speed can also affect the angular and position stability of the antennas and, thus, result in pointing errors [3]. Despite pointing errors being an important factor to be considered in many studies, it should be mentioned that including them jointly in general fading models makes the performance analysis more difficult. Thus, the search over the years for realistic and simple fading models, written in terms of physical parameters, able to characterize many effects and that can adhere well to measured data becomes a relevant, complex task and is a great challenge for the researchers.

From this motivation, this work presents a general composite fading model, namely α-$\mathcal{F}$ distribution with pointing errors. This new model jointly characterizes the deterministic path loss, the stochastic fading due to the multipath, shadowing, nonlinearity of the medium, and the antenna pointing errors. This evidences the usefulness and capability of the α-$\mathcal{F}$ distribution with pointing errors, making it suitable for applications in practical and emerging wireless scenarios, such as multihop, reconfigurable intelligent surface (RIS), and non-orthogonal multiple access (NOMA) systems.

1.2 RELATED WORKS

Recent works are described in the literature where the misalignment is adopted in different contexts, such as single-hop [2, 4, 5], dual-hop [6], multiple-input multiple-output (MIMO) [7] and NOMA-THz [8] transmission systems, free space optics (FSO) [9] and RIS [10], for example. In [5], an analytical framework is presented in order to evaluate the joint effect of misalignment and hardware imperfections in the presence of multipath fading, modeled by the α-μ distribution, in a THz wireless fiber extenders system. In [4], an analysis is fulfilled about THz communications over α-μ fading channels under random fog conditions with misalignment. In the mentioned analysis, expressions written in terms of I-function [11] for the probability density function (PDF) and cumulative distribution function (CDF) of the instantaneous signal-to-noise ratio (SNR) are derived and employed to obtain novel closed-form expressions for metrics such as outage probability (OP), average bit error probability (BEP) and average ergodic capacity. It should be mentioned that the I-function is not available in well-known software packages such as MATLAB and MATHEMATICA. In [12], a performance analysis of a multihop THz wireless system over mixed channel fading with shadowing and antenna misalignment is presented. The $N+1$-hop THz system consists of an N-hop backhaul link and a single-hop shadowed radio access link over the THz band. The researchers adopt the α-μ fading distribution to characterize the multihop link and the composite generalized-K shadowed fading for modeling the radio access link. Closed-form expressions and bounds for important statistics are shown in [12]. In addition, the impact of multiple relays in the backhaul link is evaluated by means of the OP and BEP. An asymptotic analysis is also provided in [12].

Expressions are derived in [10] for many statistics and metrics under RIS-aided THz wireless systems under α-μ fading channels with pointing errors. An RIS-assisted THz system under pointing errors and random phase noise is analyzed in [13]. From the derived statistical results, exact and asymptotic expressions are also presented in [13]. Several theoretical curves are shown considering pointing errors and validated using Monte-Carlo simulations. Performance analysis of an RIS-assisted THz wireless communication system is evaluated in [14] by means of closed-form upper bounded ergodic capacity and OP expressions. The authors in [14] consider not only the RIS reflected channels but also the direct channel between the communication nodes. Another study about RIS-assisted THz wireless systems under pointing errors is shown in [15],

where the THz channel is assumed to follow the κ-μ shadowed fading model. Approximations are also presented for the statistics, and exact expressions are deduced for the OP, ergodic capacity, and BEP.

Experimental works concerning THz wireless links are also presented in the literature, such as [16, 17]. In [16], fitting results are presented of α-μ, Nakagami-m, Rice, and log-normal distributions to the small-scale fading of THz wireless channel measurements, where the α-μ provided the best adherence. Additionally, the performance of the ergodic capacity is assessed. In [17], a measurement campaign is also conducted by the same authors of [16], considering various line-of-sight (LoS) and non-LoS links, in which the α-μ distribution is fitted to experimental THz channel gain measurements. In [16, 17], shadowing is not considered. However, as reported in [18], shadowing is an important factor to be analyzed in THz systems.

In the literature, NOMA has been investigated over downlink and uplink scenarios under fading and beam misalignment. The performance of NOMA downlink systems under single [19] and cascaded [20] Nakagami-m fading channels is presented in the literature. Expressions for the pairwise error probability (PEP), as well as an exact union bound on the bit error rate (BER), are derived in [19] under imperfect successive interference cancellation (SIC). Several expressions for the first-order statistics, ergodic channel capacity, and PEP are deduced in [20]. The performance of NOMA-based vehicular networks over α-μ fading channels is presented in [21] considering imperfect SIC, employing closed-form and asymptotic PEPs, under residual hardware impairment and outdated and imperfect channel state information. Another work under α-μ fading channels is presented in [22], where a performance analysis for downlink NOMA systems is made through closed-form OP, BER, and ergodic capacity expressions.

The design of THz-NOMA in the presence of beam misalignment is proposed in [23]. In [24], joint beam management and power allocation in THz-NOMA networks are studied. In [25], the FSO/THz-radio frequency (RF) dual-hop downlink NOMA-based is proposed, where closed-form expressions are derived for the OP and ergodic capacity under single-user and NOMA systems. A survey on error rate analysis of NOMA has been presented in [26].

1.3 ORIGINAL CONTRIBUTIONS

This manuscript is based on the work presented in papers published in top journals in the field of this dissertation. It contains original contributions to the state-of-the-art, namely:

- Chapter 2 presents: (i) a study about the α-$\mathcal{F}$ distribution with pointing errors, in which new closed-form expressions are derived for the PDF, CDF, higher-order moments, and moment generating function (MGF) of the instantaneous SNR; (ii) new expressions for OP, symbol error probability (SEP), and ergodic channel capacity; (iii) asymptotic expressions in order to provide insights into the effect of the channel and pointing error parameters on the system performance; (iv) an application of the α-$\mathcal{F}$ model with pointing errors over a RIS-assisted wireless emerging system.

- Cascaded and the sum of cascaded α-$\mathcal{F}$ fading distribution with pointing errors is studied in Chapter 3 for the first time. The main contributions of the mentioned chapter are: (i) new closed-form expressions are deduced for the PDF, CDF, and MGF of the instantaneous SNR, considering the cascaded and the sum of cascaded α-$\mathcal{F}$ fading with pointing errors; (ii) new expressions are obtained for OP, BEP, ergodic channel capacity, and area under the receiver operating characteristics (AUC), under cascaded α-$\mathcal{F}$ fading with pointing errors; (iii) a new OP expression is obtained for the sum of cascaded α-$\mathcal{F}$ fading with pointing errors which is used to assess the performance of RIS-assisted systems; and (iv) asymptotic expressions are also deduced to provide insights into the effect of the channel and pointing error parameters on the system performance at a high SNR regime.

- The performance of NOMA under multipath, shadowing, non-linearity and pointing error impairment is presented in Chapter 4, with the following contributions: i) new and exact expressions are derived for the PDF of the instantaneous SNR of the l-th user; (ii) closed-form and asymptotic expressions are derived for the PEP under imperfect SIC, considering an arbitrary number of users and (iii) the achievable theoretical diversity gains and the bit error rate (BER) union bound are shown.

1.4 PUBLICATIONS

1. P. H. D. Almeida et al. The α-$\mathcal{F}$ composite distribution with pointing errors: theory and applications to RIS. *Journal of Franklin Institute*, vol. 361, no. 10, pp. 1-13, May 2024.

2. P. H. D. Almeida et al. Cascaded and sum of cascaded over α–$\mathcal{F}$ fading channels with pointing error impairment. *IEEE Open Journal of Vehicular Technology*, vol. 5, pp. 752-761, May 2024.

3. P. H. D. Almeida et al. On the performance of NOMA systems under α-$\mathcal{F}$ channels with beam misalignment. *IEEE Wireless Communications Letters*, Under Review, Sep. 2024.

1.5 DOCUMENT ORGANIZATION

This document is organized into four chapters, described as follows: Chapter 1 starts by recalling the scope and motivation of this study. Furthermore, provides the start-of-the-art concerning works that deal with fading and misalignment in different contexts. Finally, the structure of this document is presented.

Chapter 2 presents the α-$\mathcal{F}$ fading distribution with pointing errors, in which new expressions for relevant statistics and metrics are derived. An application of the mentioned model under RIS-assisted wireless system is also shown.

Chapter 3 introduces and mathematically characterizes the cascaded and the sum of cascaded α-$\mathcal{F}$ fading distribution with pointing errors. Exact and new closed-form and asymptotic expressions for important statistics and metrics are presented in order to analyze these effects and design parameters in the technical THz literature.

Chapter 4 shows the performance of NOMA systems over α-$\mathcal{F}$ distribution with beam misalignment. New and exact expressions are derived for statistics and metrics under arbitrary number of users. Furthermore, the achievable theoretical diversity gains and the BER union bound are analyzed. Several PEP curves are presented under different channel conditions.

CHAPTER 2

THE α-$\mathcal{F}$ COMPOSITE FADING DISTRIBUTION WITH POINTING ERRORS

Outline

The α-$\mathcal{F}$ fading distribution with pointing errors is introduced in this chapter, where several statistics and metrics are derived. To the best of author knowledge, no work addresses the aforementioned model in the literature. All expressions deduced are new and generalist, with applications in different emerging scenarios, such as RIS and THz system.

2.1 SYSTEM AND CHANNEL MODELS

The received signal can be written as

$$Y = h_{\mathrm{l}} H_{\mathrm{f}} H_{\mathrm{p}} X + W, \tag{2.1}$$

in which X is the transmitted signal, W is the additive white Gaussian noise, H_{f} denotes the composite fading channel, H_{p} represents the misalignment component, and h_{l} is the path loss, that is constant for a given weather condition and link distance. For THz systems, $h_{\mathrm{l}} = h_{\mathrm{fl}} h_{\mathrm{al}}$, where h_{fl} models the propagation gain and is given by $h_{\mathrm{fl}} = c\sqrt{G_t G_r}/\left(4\pi f d\right)$, in which G_t and G_r are, respectively, the gains of the transmit and receive antenna. Furthermore, c is the speed of light, f is the operating frequency, and d is the distance between the transmitter and the receiver. In addition, h_{al} characterizes the molecular absorption gain and is given by $h_{\mathrm{al}} = \exp\left(-\kappa(f)d/2\right)$, in which $\kappa(f)$ denotes the absorption coefficient. More details about h_{l} can be found in [2].

The fading channel is characterized by the α-$\mathcal{F}$ composite distribution with the envelope PDF given by [27, Eq. (1)]

$$f_{H_{\mathrm{f}}}(h_{\mathrm{f}}) = \frac{\alpha h_{\mathrm{f}}^{\alpha\mu-1}}{\mathrm{B}(\mu,m)} \left(\frac{\hat{r}^{\alpha}}{\Psi}\right)^{m} \left(h_{\mathrm{f}}^{\alpha} + \frac{\hat{r}^{\alpha}}{\Psi}\right)^{-(\mu+m)}, \tag{2.2}$$

where $\Psi = \mu/(m-1)$, $\hat{r} = \sqrt[\alpha]{\mathbb{E}[H_{\mathrm{f}}^{\alpha}]}$ denotes the α-root mean value, α characterizes the non-linearity of the propagation medium, μ represents the number of multipath clusters, m is the shadowing parameter and $\mathrm{B}(\cdot,\cdot)$ is the Beta function [28, Eq. (06.18.02.0001.01)]. In this study, the α-$\mathcal{F}$ distribution [29] is adopted to model the fading channel since its statistics are simple and written in terms of physical parameters. The α-$\mathcal{F}$ is a fading model that jointly considers the short-term fading (α-μ) and the long-term fading ($\mathcal{F}$ distribution) of a wireless fading channel. In other words, the α-$\mathcal{F}$ is the α-μ shadowed distribution. The model mentioned is supported by experimental results [29], and it is adopted in many works under different real-world scenarios [30, 31, 32, 33]. Note that the α-$\mathcal{F}$ distribution includes other well-known distributions as special cases, such as the α-μ ($m \to \infty$) and the Fisher-Snedecor $\mathcal{F}$ ($\alpha = 2$) distributions–and their inclusive ones. It should be mentioned that the α-$\mathcal{F}$ composite fading model considers small and large-scale fading, as well as the non-linearity of the medium [29]. This indicates the potential of employing the α-$\mathcal{F}$ distribution to characterize THz channels.

The pointing error PDF impairment is given by [2, Eq. (22)]

$$f_{H_{\mathrm{p}}}(h_{\mathrm{p}}) = z^2 A_0^{-z^2} h_{\mathrm{p}}^{z^2-1},\ 0 \leq h_{\mathrm{p}} \leq A_0, \tag{2.3}$$

in which A_0 is the fraction of the collected power and $z = \omega_{\mathrm{eq}}/2\sigma$ is the ratio between the equivalent beam radius at the receiver and the pointing error displacement standard deviation [34]. For $z \to \infty$, it should be mentioned that the case of the non-pointing error is assumed. The pointing error model adopted is a realistic model and has been successfully adopted in many important papers dealing with THz systems [2, 6, 7, 8, 35], requiring only the use of circular lenses at the transmitter and receiver sides. This is important because the pointing error parameter is calculated by radial distances between the transmit and receive beams. Furthermore, the statistics of the mentioned distribution are exact and simple. The aforementioned pointing error model was adopted to quantify the impact of the beam misalignment in the system. In the literature, new pointing error models for millimeter wave and THz high-directional antennas are presented [3, 36].

2.2 STATISTICS FOR THE α-$\mathcal{F}$ COMPOSITE FADING DISTRIBUTION WITH POINTING ERRORS

Several statistics for the α-$\mathcal{F}$ composite fading model with pointing errors are derived in this section.

Proposition 2.2.1. *(PDF and CDF of the Envelope/Instantaneous SNR) – Let μ, α, $\hat{r}$, z, $\bar{\gamma}$, A_0, h_l, h, $\gamma \in \mathbb{R}^+$ and $m > 1$. The PDF and the CDF of the envelope $H = h_{\rm l}H_{\rm f}H_{\rm p}$, for the α-$\mathcal{F}$ composite fading model with pointing errors, can be obtained, respectively, as*

$$f_H(h) = \frac{z^2}{h\Gamma(\mu)\Gamma(m)} \mathrm{G}_{2,2}^{2,1}\left[\Psi\left(\frac{h}{\hat{r}h_l A_0}\right)^{\alpha} \,\middle|\, \begin{matrix} 1-m, z^2/\alpha+1 \\ \mu, z^2/\alpha \end{matrix}\right] \tag{2.4}$$

and

$$F_H(h) = \frac{z^2}{\alpha\Gamma(\mu)\Gamma(m)} \mathrm{G}_{3,3}^{2,2}\left[\Psi\left(\frac{h}{\hat{r}h_l A_0}\right)^{\alpha} \,\middle|\, \begin{matrix} 1-m, 1, z^2/\alpha+1 \\ \mu, z^2/\alpha, 0 \end{matrix}\right], \tag{2.5}$$

where $\Gamma(\cdot)$ is the Gamma function [28, Eq. (06.05.02.0001.01)] and $\mathrm{G}[\cdot]$ is the Meijer G-function [37, Eq. (9.301)]. In turn, the PDF and CDF of the instantaneous SNR, in the presence of α-$\mathcal{F}$ composite fading with pointing errors, are given respectively by

$$f_\Gamma(\gamma) = \frac{z^2}{2\gamma\Gamma(\mu)\Gamma(m)} \mathrm{G}_{2,2}^{2,1}\left[\Psi\left(\frac{z\sqrt{\gamma}}{\sqrt{\bar{\gamma}(z^2+2)}}\right)^{\alpha} \,\middle|\, \begin{matrix} 1-m, z^2/\alpha+1 \\ \mu, z^2/\alpha \end{matrix}\right], \tag{2.6}$$

and

$$F_\Gamma(\gamma) = \frac{z^2}{\alpha\Gamma(\mu)\Gamma(m)} \mathrm{G}_{3,3}^{2,2}\left[\Psi\left(\frac{z\sqrt{\gamma}}{\sqrt{\bar{\gamma}(z^2+2)}}\right)^{\alpha} \,\middle|\, \begin{matrix} 1-m, 1, z^2/\alpha+1 \\ \mu, z^2/\alpha, 0 \end{matrix}\right], \tag{2.7}$$

in which $\bar{\gamma}$ is the average SNR.

Proof. The PDF of $H = h_{\rm l}H_{\rm f}H_{\rm p}$, denoted by $f_H(h)$, can be derived by means of

$$f_H(h) = \frac{1}{h_{\rm l}} \int_0^\infty \frac{1}{v} f_{H_{\rm f}}\Big(\frac{h}{h_{\rm l}v}\Big) f_{H_{\rm p}}(v) \mathrm{d}v. \tag{2.8}$$

Substituting (2.2) and (2.3) in the expression of $f_H(h)$, performing the change of variable $t = v^{-\alpha}$ and using [37, Eq. (3.194.2)], $f_H(h)$ can be written after simplifications as

$$f_H(h) = \frac{\alpha z^2}{h\mathrm{B}(\mu,m)(\alpha m + z^2)} \left(\frac{A_0^\alpha \hat{r}^\alpha}{\Psi}\right)^m \left(\frac{h_{\rm l}}{h}\right)^{\alpha m} {}_2\mathrm{F}_1\Big[\mu+m, m+\frac{z^2}{\alpha}, m+\frac{z^2}{\alpha}+1; \, -\xi\Big], \tag{2.9}$$

in which $\xi = \hat{r}^{\alpha} h_{\mathrm{l}}^{\alpha} A_0^{\alpha}/(\Psi h^{\alpha})$ and ${}_2\mathrm{F}_1[\cdot,\cdot,\cdot;\cdot]$ is the Gauss hypergeometric function [37, Eq. (9.100)]. In the sequence, employing [38, Eq. (8.4.49.14)] and [39, Eq. (9.31.5)] and performing with some algebraic manipulations, (2.4) is obtained.

The CDF of H, $F_H(h)$, can be derived integrating (2.4), i.e,

$$F_H(h) = \frac{z^2}{\Gamma(\mu)\Gamma(m)} \int_0^h \frac{1}{x} \mathrm{G}_{2,2}^{2,1}\left[\Psi \left(\frac{x}{\hat{r} h_{\mathrm{l}} A_0} \right)^{\alpha} \middle| \begin{matrix} 1-m, z^2/\alpha+1 \\ \mu, z^2/\alpha \end{matrix} \right] \mathrm{d}x. \tag{2.10}$$

Expressing the Meijer G-function of (2.10) in terms of the Mellin-Barnes integral, the innermost integral in the variable x is of the power-type and can be solved. In addition, using $\Gamma(x+1) = x\Gamma(x)$ and the definition of the Meijer G-function, (2.5) is derived. Hence, the proof is complete.

Making $\Gamma = H^2$, the PDF of the instantaneous SNR can be obtained by means of

$$f_{\Gamma}(\gamma) = \frac{1}{2\sqrt{\gamma}} f_H(\sqrt{\gamma}). \tag{2.11}$$

Using (2.4), (2.6) is easily deduced. Furthermore, $F_{\Gamma}(\gamma)$ is derived from (2.5), since $F_{\Gamma}(\gamma) = F_H(\sqrt{\gamma})$. The result for $F_{\Gamma}(\gamma)$ is presented in (2.7) and completes the proof. □

Proposition 2.2.2. *(Higher-order Moments of the Instantaneous SNR) – For μ, α, $\bar{\gamma}$, z, $h_l \in \mathbb{R}^+$ and $n \in \mathbb{N}^+$, the higher-order moments of the instantaneous SNR over the α-$\mathcal{F}$ composite fading model with pointing errors, is obtained as*

$$\mathbb{E}[\gamma^n] = \frac{z^2 \Gamma(\mu + \frac{2n}{\alpha}) \Gamma(m - \frac{2n}{\alpha})}{(z^2+2n)\Gamma(\mu)\Gamma(m)} \left(\frac{\sqrt{\bar{\gamma}(z^2+2)}}{z \Psi^{\frac{1}{\alpha}}} \right)^{2n}, \tag{2.12}$$

which is valid for $m > 2n/\alpha$.

Proof. The higher-order moments of the instantaneous SNR, $\mathbb{E}[\gamma^n]$, is calculated as

$$\mathbb{E}[\gamma^n] = \int_0^{\infty} \gamma^n f_{\Gamma}(\gamma) \mathrm{d}\gamma. \tag{2.13}$$

Substituting (2.6),

$$\mathbb{E}[\gamma^n] = \frac{z^2}{2\Gamma(\mu)\Gamma(m)} \int_0^{\infty} \frac{\gamma^n}{\gamma} \mathrm{G}_{2,2}^{2,1}\left[\Psi \left(\frac{z\sqrt{\gamma}}{\sqrt{\bar{\gamma}(z^2+2)}} \right)^{\alpha} \middle| \begin{matrix} 1-m, z^2/\alpha+1 \\ \mu, z^2/\alpha \end{matrix} \right] \mathrm{d}\gamma. \tag{2.14}$$

Performing the variable change $x = \gamma^{\alpha/2}$, using [37, Eq. (7.811.4)] and making some algebraic manipulations, (2.12) is derived, that complete the proof. □

Proposition 2.2.3. *(MGF of the Instantaneous SNR) – Let μ, α, $\bar{\gamma}$, z, h_l, $s \in \mathbb{R}^+$ and $m > 1$. The MGF of the instantaneous SNR over the α-$\mathcal{F}$ composite fading model with pointing errors is given by*

$$\mathrm{M}_{\Gamma}(s) = \frac{z^2}{2\Gamma(\mu)\Gamma(m)} \mathrm{H}_{3,2}^{2,2}\left[\left(\frac{z\Psi^{\frac{1}{\alpha}}}{\sqrt{s\bar{\gamma}(z^2+2)}} \right)^{\alpha} \middle| \begin{matrix} (1-m,1),(1,\frac{\alpha}{2}),(\frac{z^2}{\alpha}+1,1) \\ (\mu,1),(\frac{z^2}{\alpha},1) \end{matrix} \right], \tag{2.15}$$

with $\mathrm{H}[\cdot]$ *denoting the Fox H-function [39, Eq. (1.2)].*

Proof. The MGF is defined as

$$\mathrm{M}_{\Gamma}(s) = \int_0^{\infty} f_{\Gamma}(\gamma) \exp(-s\gamma) \mathrm{d}\gamma. \tag{2.16}$$

Replacing (2.6), using [28, 07.34.26.0008.01], [28, 01.03.26.0004.01] and [40, Eq. (2.8.4)], (2.15) can be obtained after simplifications. Hence, the proof is complete. □

2.3 PERFORMANCE ANALYSIS

2.3.1 Outage Probability

The OP, P_{out}, is defined as the point at which the SNR at the output of the receiver falls below a threshold γ_{th}. Mathematically, by using (2.7), $P_{\text{out}} = F_{\Gamma}(\gamma_{\text{th}})$.

2.3.2 Symbol Error Probability

The average SEP, P_{sym}, can be evaluated as [41, Eq. (7)]

$$P_{\text{sym}} = \frac{\theta}{2\sqrt{2\pi}} \int_0^{\infty} \frac{1}{\sqrt{\gamma}} \exp\left(-\gamma/2\right) F_{\gamma}\left(\frac{\gamma}{\phi}\right) \mathrm{d}\gamma, \tag{2.17}$$

in which the parameters θ and ϕ depend on the type of modulation. Substituting (2.7) into (2.17), using [28, 07.34.26.0008.01],[28, 01.03.26.0004.01] and [40, Eq. (2.8.4)], after simplifications, the SEP is given by

$$P_{\text{sym}} = \frac{\theta z^2}{2\sqrt{\pi}\alpha\Gamma(\mu)\Gamma(m)} \mathrm{H}_{4,3}^{2,3}\left[\Psi \left(\frac{z\sqrt{2}}{\sqrt{\phi\bar{\gamma}(z^2+2)}} \right)^{\alpha} \middle| \begin{matrix} (1-m,1),(1,1),(1/2,\frac{\alpha}{2}),(\frac{z^2}{\alpha}+1,1) \\ (\mu,1),(\frac{z^2}{\alpha},1),(0,1) \end{matrix} \right]. \tag{2.18}$$

2.3.3 Channel Capacity

The channel capacity, in bps/Hz, is calculated as

$$C_{\text{erg}} = \frac{1}{\ln(2)} \int_0^{\infty} f_{\Gamma}(\gamma) \ln(1+\gamma) \mathrm{d}\gamma. \tag{2.19}$$

Replacing (2.6) in the expression of C_{erg} and using [28, 01.04.26.0003.01], [28, 07.34.26.0008.01], [28, 01.03.26.0004.01] and [40, Eq. (2.8.4)], the channel capacity can be written as

$$C_{\text{erg}} = \frac{z^2}{2\ln(2)\Gamma(\mu)\Gamma(m)} \mathrm{H}_{4,4}^{4,2}\left[\frac{z^{\alpha}\Psi}{(\bar{\gamma}(z^2+2))^{\alpha/2}} \middle| \begin{matrix} (1-m,1),(0,\frac{\alpha}{2}),(1,\frac{\alpha}{2}),(\frac{z^2}{\alpha}+1,1) \\ (\mu,1),(\frac{z^2}{\alpha},1),(0,\frac{\alpha}{2}),(0,\frac{\alpha}{2}) \end{matrix} \right]. \tag{2.20}$$

2.4 ASYMPTOTIC ANALYSIS

2.4.1 Asymptotic Outage Probability

For $\bar{\gamma} \to \infty$, the asymptotic OP can be derived by means of (2.7), using [28, 07.34.26.0008.01] and [40, Theorem 1.11], in which only the dominant term is considered. After simplifications, P_{out}^{∞} is written as

$$P_{\text{out}}^{\infty} = \begin{cases} \frac{z^2\Psi^{\mu}}{(z^2\mu-\alpha\mu^2)\mathrm{B}(\mu,m)} \left(\frac{\sqrt{\bar{\gamma}(z^2+2)}}{z\sqrt{\gamma_{\text{th}}}} \right)^{-\alpha\mu} & , \alpha\mu < z^2 \\ \frac{\Gamma(\mu-\frac{z^2}{\alpha})\Gamma(m+\frac{z^2}{\alpha})}{\Gamma(\mu)\Gamma(m)\Psi^{-\frac{z^2}{\alpha}}} \left(\frac{\sqrt{\bar{\gamma}(z^2+2)}}{z\sqrt{\gamma_{\text{th}}}} \right)^{-z^2} & , \alpha\mu > z^2 \end{cases}. \tag{2.21}$$

In high SNRs values, $P_{\text{out}}^{\infty} \sim \bar{\gamma}^{-G_{\text{d}}}$, where G_{d} is the diversity order/gain. From (2.21), it is noted that $G_{\text{d}} = \min(\alpha\mu/2, z^2/2)$. That is, the diversity order depends on the fading and pointing error parameters.

2.4.2 Asymptotic Symbol Error Probability

For $\bar{\gamma} \to \infty$, the asymptotic SEP can be deduced applying [40, Theorem 1.11] in (2.18), as given by

$$P_{\text{sym}}^{\infty} = \begin{cases} \frac{\theta z^2 \Gamma(\frac{\alpha\mu+1}{2})\Psi^{\mu}}{2\sqrt{\pi}\mu(z^2-\alpha\mu)\mathrm{B}(\mu,m)} \left(\frac{\sqrt{\bar{\gamma}\phi(z^2+2)}}{z\sqrt{2}} \right)^{-\alpha\mu} & , \alpha\mu < z^2 \\ \frac{\theta\Gamma(\mu-\frac{z^2}{\alpha})\Gamma(m+\frac{z^2}{\alpha})\Gamma(\frac{1+z^2}{2})}{2\sqrt{\pi}\Gamma(\mu)\Gamma(m)\Psi^{-\frac{z^2}{\alpha}}} \left(\frac{\sqrt{\bar{\gamma}\phi(z^2+2)}}{z\sqrt{2}} \right)^{-z^2} & , \alpha\mu > z^2 \end{cases} \tag{2.22}$$

after some algebraic manipulations. In (2.22), if only the dominant term is considered then $G_{\text{d}} = \min(\alpha\mu/2, z^2/2)$.

2.4.3 Asymptotic Ergodic Capacity

The asymptotic ergodic capacity at high SNR values is given by [42]

$$C_{\text{erg}}^{\infty} = \log_2(\bar{\gamma}) + \log_2(e)\frac{\partial}{\partial n}\frac{\mathbb{E}[\gamma^n]}{\bar{\gamma}^n}\bigg|_{n=0}, \tag{2.23}$$

in which $\partial/\partial n$ is the first derivative operator.

The term $\frac{\partial}{\partial n}\frac{\mathbb{E}[\gamma^n]}{\bar{\gamma}^n}$ in (2.23) can be written as

$$\frac{\partial}{\partial n}\frac{\mathbb{E}[\gamma^n]}{\bar{\gamma}^n} = \frac{\partial}{\partial n}\frac{\mathbb{E}[\gamma^n]}{\exp(n\ln(\bar{\gamma}))} = -\ln(\bar{\gamma})\mathbb{E}[\gamma^n]\exp(-n\ln(\bar{\gamma})) + \exp(-n\ln(\bar{\gamma}))\frac{\partial}{\partial n}\mathbb{E}[\gamma^n]. \tag{2.24}$$

Substituting (2.24) in (2.23), C_{erg}^{∞} can be written after simplifications as

$$C_{\text{erg}}^{\infty} = \log_2(\bar{\gamma}) - \log_2(e)\ln(\bar{\gamma}) + \log_2(e)\frac{\partial}{\partial n}\mathbb{E}[\gamma^n]\bigg|_{n=0}. \tag{2.25}$$

Using (2.12),

$$\begin{aligned}\frac{\partial}{\partial n}\mathbb{E}\left[\gamma^n\right] = &-\frac{2}{z^2+2n}\mathbb{E}[\gamma^n] + \frac{2}{\alpha}\mathbb{E}[\gamma^n]\frac{\Gamma'\left(\mu+2n/\alpha\right)}{\Gamma\left(\mu+2n/\alpha\right)} - \frac{2}{\alpha}\mathbb{E}[\gamma^n]\frac{\Gamma'\left(m-2n/\alpha\right)}{\Gamma\left(m-2n/\alpha\right)} \\ &+ \ln(\bar{\gamma})\mathbb{E}[\gamma^n] + 2\mathbb{E}[\gamma^n]\ln\left[\frac{\sqrt{z^2+2}}{z}\left(\frac{1}{\Psi}\right)^{\frac{1}{\alpha}}\right].\end{aligned} \tag{2.26}$$

Replacing (2.26) in (2.25) and proceeding with simplifications,

$$C_{\text{erg}}^{\infty} = \log_2(\overline{\gamma}) + 2\log_2(e)\left[\frac{\psi(\mu)}{\alpha} - \frac{\psi(m)}{\alpha} - \frac{1}{z^2} + \ln\left(\frac{\sqrt{z^2+2}}{z}\Big(\frac{1}{\Psi}\Big)^{\frac{1}{\alpha}}\right)\right], \tag{2.27}$$

with $\psi(x) = \Gamma'(x)/\Gamma(x)$ is the digamma function [37, Eq. (8.36)].

2.5 RIS-AIDED WIRELESS SYSTEM OVER α-$\mathcal{F}$ FADING WITH POINTING ERRORS

This section considers a RIS-aided system over α-$\mathcal{F}$ fading with pointing errors, which is a new and emerging wireless scenario. In this application, the RIS is composed of L elements, and the received signal is given by

$$Y = \sum_{i=1}^{L} H_{i,1}H_{i,2}X + W, \tag{2.28}$$

where X is the transmitted signal, W is the zero-mean_σ^2-variance additive white Gaussian noise and $H_{i,1}$ and $H_{i,2}$ are the fading gains between the source and the i-th RIS element and between the i-th RIS element and the destination, respectively. Here, it is assumed that the phases of $H_{i,1}$ and $H_{i,2}$ are known and can be perfectly compensated at the RIS. This assumption of perfect channel state information has been widely used in the literature to maximize the received SNR [43, 44, 45].

Proposition 2.5.1. *(PDF, CDF, and MGF of the Instantaneous SNR) –The PDF, CDF, and MGF of the instantaneous SNR, under a sum of double α-$\mathcal{F}$ random variates with pointing errors, are given respectively by*

$$f_\Gamma(\gamma) = \frac{1}{2\gamma}\left[\prod_{i=1}^{L}\prod_{j=1}^{2}\frac{z_{i,j}^2}{\alpha_{i,j}\Gamma(\mu_{i,j})\Gamma(m_{i,j})}\right] \times \mathrm{H}_{0,1:[5,4]_{i=1:L}}^{0,0:[4,3]_{i=1:L}}\left[\begin{array}{c|c|c} \Xi_1\sqrt{\gamma} & - & [(1,1),\mathcal{A}_{i,1},\mathcal{A}_{i,2},\mathcal{B}_{i,1},\mathcal{B}_{i,2}]_{i=1:L} \\ \vdots & (1;\{1\}_{i=1:L}) & [\mathcal{C}_{i,1},\mathcal{C}_{i,2},\mathcal{D}_{i,1},\mathcal{D}_{i,2}]_{i=1:L} \\ \Xi_L\sqrt{\gamma} & & \end{array}\right], \tag{2.29}$$

$$F_\Gamma(\gamma) = \frac{1}{2}\left[\prod_{i=1}^{L}\prod_{j=1}^{2}\frac{z_{i,j}^2}{\alpha_{i,j}\Gamma(\mu_{i,j})\Gamma(m_{i,j})}\right] \times \mathrm{H}_{1,2:[5,4]_{i=1:L}}^{0,1:[4,3]_{i=1:L}}\left[\begin{array}{c|c|c} \Xi_1\sqrt{\gamma} & \left(1;\{\frac{1}{2}\}_{i=1:L}\right) & [(1,1),\mathcal{A}_{i,1},\mathcal{A}_{i,2},\mathcal{B}_{i,1},\mathcal{B}_{i,2}]_{i=1:L} \\ \vdots & (1;\{1\}_{i=1:L}),\left(0;\{\frac{1}{2}\}_{i=1:L}\right) & [\mathcal{C}_{i,1},\mathcal{C}_{i,2},\mathcal{D}_{i,1},\mathcal{D}_{i,2}]_{i=1:L} \\ \Xi_L\sqrt{\gamma} & & \end{array}\right] \tag{2.30}$$

and

$$\mathrm{M}_\Gamma(s) = \frac{1}{2}\left[\prod_{i=1}^{L}\prod_{j=1}^{2}\frac{z_{i,j}^2}{\alpha_{i,j}\Gamma(\mu_{i,j})\Gamma(m_{i,j})}\right] \times \mathrm{H}_{1,1:[5,4]_{i=1:L}}^{0,1:[4,3]_{i=1:L}}\left[\begin{array}{c|c|c} \frac{\Xi_1}{(-s)^{\frac{1}{2}}} & \left(1;\{\frac{1}{2}\}_{i=1:L}\right) & [(1,1),\mathcal{A}_{i,1},\mathcal{A}_{i,2},\mathcal{B}_{i,1},\mathcal{B}_{i,2}]_{i=1:L} \\ \vdots & (1;\{1\}_{i=1:L}) & [\mathcal{C}_{i,1},\mathcal{C}_{i,2},\mathcal{D}_{i,1},\mathcal{D}_{i,2}]_{i=1:L} \\ \frac{\Xi_L}{(-s)^{\frac{1}{2}}} & & \end{array}\right], \tag{2.31}$$

in which $\mathcal{A}_{i,j} = (1-m_{i,j},1/\alpha_{i,j})$, $\mathcal{B}_{i,j} = \left(\frac{z_{i,j}^2}{\alpha_{i,j}}+1,1/\alpha_{i,j}\right)$, $\mathcal{C}_{i,j} = (\mu_{i,j},1/\alpha_{i,j})$, $\mathcal{D}_{i,j} = \left(\frac{z_{i,j}^2}{\alpha_{i,j}},1/\alpha_{i,j}\right)$ *and*

$$\Xi_i = \prod_{j=1}^{2}\frac{\Psi_{i,j}^{1/\alpha_{i,j}} z_{i,j}}{\sqrt{\bar{\gamma}_{i,j}(z_{i,j}^2+2)}}. \tag{2.32}$$

Proof. Let $X = H_1H_2$, where $f_{H_j}(t)$, with $j = 1, 2$, is given by (2.4). The Mellin transform of $f_{H_j}(t)$, denoted by $\mathcal{M}[f_{H_j}(t)]$, can derived using [39, Eq. (2.9)] and making the variable change

$y = t^{\alpha_j}$. After simplifications,

$$\mathcal{M}[f_{H_j}(t)] = \frac{z_j^2}{\alpha_j \Gamma(\mu_j)\Gamma(m_j)} \left[\frac{\Psi_j}{\left(\hat{r}_j h_{l_j} A_{0_j}\right)^{\alpha_j}}\right]^{\frac{(1-s)}{\alpha_j}} \times \frac{\Gamma\left(\mu_j + \frac{(s-1)}{\alpha_j}\right)\Gamma\left(\frac{z_j^2}{\alpha_j} + \frac{(s-1)}{\alpha_j}\right)\Gamma\left(1-(1-m_j)-\frac{(s-1)}{\alpha_j}\right)}{\Gamma\left(\frac{z_j^2}{\alpha_j}+1+\frac{(s-1)}{\alpha_j}\right)}, \; j = 1{,}2. \tag{2.33}$$

According to [46, Eq. (3.5)], $\mathcal{M}[f_X(x)] = \mathcal{M}[f_{H_1}(t)]\mathcal{M}[f_{H_2}(v)]$, and the PDF of X can be deduced using [46, Eq. (3.2)]

$$f_X(x) = \frac{1}{2\pi j}\int_{\mathcal{C}} x^{-s}\mathcal{M}[f_X(x)]\mathrm{d}s, \tag{2.34}$$

that is written after simplifications as

$$f_X(x) = \prod_{j=1}^{2} \frac{z_j^2 \Psi_j^{1/\alpha_j}}{\alpha_j \Gamma(\mu_j)\Gamma(m_j)\hat{r}_j h_{l_j} A_{0_j}} \mathrm{H}_{4,4}^{4,2}\left[x\prod_{j=1}^{2}\frac{\Psi_j^{1/\alpha_j}}{\hat{r}_j h_{l_j} A_{0_j}}\middle| \begin{matrix}\Phi_1,\Phi_2,\Theta_1,\Theta_2\\ \Upsilon_1,\Upsilon_2,\Omega_1,\Omega_2\end{matrix}\right], \tag{2.35}$$

in which $\Phi_j = \left(1-m_j-\frac{1}{\alpha_j},\frac{1}{\alpha_j}\right)$, $\Upsilon_j = \left(\mu_j-\frac{1}{\alpha_j},\frac{1}{\alpha_j}\right)$, $\Theta_j = \left(\frac{z_j^2-1}{\alpha_j}+1,\frac{1}{\alpha_j}\right)$ and $\Omega_j = \left(\frac{z_j^2-1}{\alpha_j},\frac{1}{\alpha_j}\right)$.

In turn, the MGF of X can be calculated as

$$\mathrm{M}_X(t) = \int_0^\infty f_X(x)\exp(-tx)dx\Big|_{(-t)}. \tag{2.36}$$

Substituting (2.35) in (2.36), using [37, Eq. (8.315.1)] and [39, Eq. (1.60)] in sequence, it follows that

$$\mathrm{M}_X(t) = \prod_{j=1}^{2}\frac{z_j^2}{\alpha_j\Gamma(\mu_j)\Gamma(m_j)}\mathrm{H}_{5,4}^{4,3}\left[\frac{1}{(-t)}\prod_{j=1}^{2}\frac{\Psi_j^{1/\alpha_j}}{\hat{r}_j h_{l_j}A_{0_j}}\middle| \begin{matrix}(1,1),\mathcal{A}_1,\mathcal{A}_2,\mathcal{B}_1,\mathcal{B}_2\\ \mathcal{C}_1,\mathcal{C}_2,\mathcal{D}_1,\mathcal{D}_2\end{matrix}\right]. \tag{2.37}$$

Defining $R = \sum_{i=1}^{L}|H_{i,1}||H_{i,2}| = \sum_{i=1}^{L}\prod_{j=1}^{2}|H_{i,j}|$, it follows that $\mathrm{M}_R(t) = \prod_{i=1}^{L}\mathrm{M}_{X_i}(t)$. Using the definition of the multivariate Fox H-function [39, Eq. (A.1)], $\mathrm{M}_R(t)$ can be written as

$$\mathrm{M}_R(t) = \left[\prod_{i=1}^{L}\prod_{j=1}^{2}\frac{z_{i,j}^2}{\alpha_{i,j}\Gamma(\mu_{i,j})\Gamma(m_{i,j})}\right] \times \mathrm{H}_{0,0:[5,4]_{i=1:L}}^{0,0:[4,3]_{i=1:L}}\left[\begin{matrix}\frac{\chi_1}{(-t)}\\ \vdots\\ \frac{\chi_L}{(-t)}\end{matrix}\middle|\begin{matrix}-\\ -\end{matrix}\middle|\begin{matrix}[(1,1),\mathcal{A}_{i,1},\mathcal{A}_{i,2},\mathcal{B}_{i,1},\mathcal{B}_{i,2}]_{i=1:L}\\ [\mathcal{C}_{i,1},\mathcal{C}_{i,2},\mathcal{D}_{i,1},\mathcal{D}_{i,2}]_{i=1:L}\end{matrix}\right], \tag{2.38}$$

in which

$$\chi_i = \prod_{j=1}^{2}\frac{\Psi_{i,j}^{1/\alpha_{i,j}}}{\hat{r}_{i,j}h_{l_{i,j}}A_{0_{i,j}}}. \tag{2.39}$$

From (2.38), the PDF of R can be calculated as

$$f_R(r) = \frac{1}{2\pi j}\int_{\mathcal{C}} \mathrm{M}_R(t)\exp(st)dt\Big|_{(-r)}. \tag{2.40}$$

Using [37, Eq. (8.315.1)] and after algebraic simplifications,

$$f_R(r) = \frac{1}{r}\left[\prod_{i=1}^{L}\prod_{j=1}^{2}\frac{z_{i,j}^2}{\alpha_{i,j}\Gamma(\mu_{i,j})\Gamma(m_{i,j})}\right] \times \mathrm{H}_{0,1:[5,4]_{i=1:L}}^{0,0:[4,3]_{i=1:L}}\left[\begin{array}{c|c|c} \chi_1 r \\ \vdots & - \\ \chi_L r & (1;\{1\}_{i=1:L}) \end{array}\middle|\begin{array}{c} [(1,1),\mathcal{A}_{i,1},\mathcal{A}_{i,2},\mathcal{B}_{i,1},\mathcal{B}_{i,2}]_{i=1:L} \\ [\mathcal{C}_{i,1},\mathcal{C}_{i,2},\mathcal{D}_{i,1},\mathcal{D}_{i,2}]_{i=1:L} \end{array}\right]. \tag{2.41}$$

Integrating (2.41),

$$F_R(r) = \left[\prod_{i=1}^{L}\prod_{j=1}^{2}\frac{z_{i,j}^2}{\alpha_{i,j}\Gamma(\mu_{i,j})\Gamma(m_{i,j})}\right] \times \mathrm{H}_{0,1:[5,4]_{i=1:L}}^{0,0:[4,3]_{i=1:L}}\left[\begin{array}{c|c|c} \chi_1 r \\ \vdots & - \\ \chi_L r & (0;\{1\}_{i=1:L}) \end{array}\middle|\begin{array}{c} [(1,1),\mathcal{A}_{i,1},\mathcal{A}_{i,2},\mathcal{B}_{i,1},\mathcal{B}_{i,2}]_{i=1:L} \\ [\mathcal{C}_{i,1},\mathcal{C}_{i,2},\mathcal{D}_{i,1},\mathcal{D}_{i,2}]_{i=1:L} \end{array}\right]. \tag{2.42}$$

Making $\Gamma = R^2$, the PDF of the instantaneous SNR can be obtained using (2.11), as shown in (2.29). Integrating (2.29), knowing that $\int_0^{\gamma} x^{n-1}\mathrm{d}x = \gamma^n/n$, $\Gamma(\gamma+1) = \gamma\Gamma(\gamma)$ and using the definition of the multivariate H-Fox, (2.30) is obtained. Finally, the MGF is deduced by computing the Laplace transform of (2.29). Using [28, id 01.03.26.0004.01], [28, id 07.34.26.0008.01], [39, Eq. (2.8)] and [39, Eq. (A.1)], (2.31) is derived. Hence, the proof is concluded. □

It should be mentioned that the statistics presented in this section are equal to [10], with $m_s \to \infty$, and equal to [47], for $z \to \infty$. Thus, this work generalizes some results presented in [10, 47].

2.5.1 Performance Analysis

2.5.1.1 Outage Probability

The OP is given by $P_{\text{out}} = F_{\Gamma}(\gamma_{\text{th}})$, in which $F_{\Gamma}(\cdot)$ is written as (2.30).

2.5.1.2 Bit Error Probability

The average bit error probability (BEP), P_{b}, can be evaluated as [48]

$$P_{\mathrm{b}} = \frac{1}{\pi}\int_0^{\frac{\pi}{2}} \mathrm{M}_{\Gamma}\left(\frac{\rho}{\sin^2\theta}\right)\mathrm{d}\theta, \tag{2.43}$$

in which ρ depends on the type of modulation considered.

Substituting (2.31) in (2.43), employing [39, Eq. (A.1)] and performing the change of variable $x = \sin^2\theta$, and using [37, Eq. (3.191.3)/Eq. (8.384.1)] in sequence, it follows that the BEP can be written in closed-form, after simplifications, as

$$P_{\mathrm{b}} = \frac{1}{4\sqrt{\pi}}\left[\prod_{i=1}^{L}\prod_{j=1}^{2}\frac{z_{i,j}^2}{\alpha_{i,j}\Gamma(\mu_{i,j})\Gamma(m_{i,j})}\right] \times \mathrm{H}_{2,2:[5,4]_{i=1:L}}^{0,2:[4,3]_{i=1:L}}\left[\begin{array}{c|c|c} \frac{\Xi_1}{\sqrt{\rho}} & \left(1;\{\frac{1}{2}\}_{i=1:L}\right),\left(\frac{1}{2};\{\frac{1}{2}\}_{i=1:L}\right) & [(1,1),\mathcal{A}_{i,1},\mathcal{A}_{i,2},\mathcal{B}_{i,1},\mathcal{B}_{i,2}]_{i=1:L} \\ \vdots & \left(1;\{1\}_{i=1:L}\right),\left(0;\{\frac{1}{2}\}_{i=1:L}\right) & [\mathcal{C}_{i,1},\mathcal{C}_{i,2},\mathcal{D}_{i,1},\mathcal{D}_{i,2}]_{i=1:L} \\ \frac{\Xi_L}{\sqrt{\rho}} & & \end{array}\right]. \tag{2.44}$$

2.5.2 Asymptotic Analysis

From (2.30) and (2.44) respectively, and considering the approach presented in [49], it follows that the asymptotic OP and BEP expressions can be written as

$$P_{\mathrm{out}}^{\infty} = \frac{1}{2\mathcal{B}}\left[\prod_{i=1}^{L}\prod_{j=1}^{2}\frac{z_{i,j}^2}{\alpha_{i,j}\Gamma(\mu_{i,j})\Gamma(m_{i,j})}\right]\Psi(U_1,...,U_L)\prod_{i=1}^{L}\phi(U_i)\left(\Xi_i\gamma_{\mathrm{th}}^{\frac{1}{2}}\right)^{U_i} \tag{2.45}$$

and

$$P_{\mathrm{b}}^{\infty} = \frac{1}{4\sqrt{\pi}\mathcal{B}}\left[\prod_{i=1}^{L}\prod_{j=1}^{2}\frac{z_{i,j}^2}{\alpha_{i,j}\Gamma(\mu_{i,j})\Gamma(m_{i,j})}\right]\Psi(U_1,...,U_L)\prod_{i=1}^{L}\phi(U_i)\left(\Xi_i\rho^{-\frac{1}{2}}\right)^{U_i}, \tag{2.46}$$

in which $\mathcal{B} = \prod_{i=1}^{L} B_{i,c_i}$,

$$U_i = \min_{1\le j\le 4}\left\{\mu_{i,1}\alpha_{i,1}, \mu_{i,2}\alpha_{i,2}, z_{i,1}^2, z_{i,2}^2\right\}, \tag{2.47}$$

$$c_i = \arg\min_{1\le j\le 4}\left\{\mu_{i,1}\alpha_{i,1}, \mu_{i,2}\alpha_{i,2}, z_{i,1}^2, z_{i,2}^2\right\}, \tag{2.48}$$

$$\phi(U_i) = \frac{\prod\limits_{j=1,\ \mu_{i,j}\neq\frac{U_i}{\alpha_{i,j}}}^{2} \Gamma\left(\mu_{i,j} - \frac{U_i}{\alpha_{i,j}}\right) \prod\limits_{j=1,\ z_{i,j}^2\neq U_i}^{2} \Gamma\left(\frac{z_{i,j}^2}{\alpha_{i,j}} - \frac{U_i}{\alpha_{i,j}}\right) \prod\limits_{j=1}^{2} \Gamma\left(1-(1-m_{i,j}) + \frac{U_i}{\alpha_{i,j}}\right) \Gamma(U_i)}{\prod\limits_{j=1}^{2} \Gamma\left(\frac{z_{i,j}^2}{\alpha_{i,j}} + 1 - \frac{U_i}{\alpha_{i,j}}\right)}, \tag{2.49}$$

$$\Psi(U_1, ..., U_L) = \frac{\Gamma\left(\sum_{i=1}^{L} \frac{1}{2} U_i\right)}{\Gamma\left(\sum_{i=1}^{L} U_i\right) \Gamma\left(1 + \sum_{i=1}^{L} \frac{1}{2} U_i\right)} \tag{2.50}$$

for the OP and

$$\Psi(U_1, ..., U_L) = \frac{\Gamma\left(\sum_{i=1}^{L} \frac{1}{2} U_i\right) \Gamma\left(\frac{1}{2} + \sum_{i=1}^{L} \frac{1}{2} U_i\right)}{\Gamma\left(\sum_{i=1}^{L} U_i\right) \Gamma\left(1 + \sum_{i=1}^{L} \frac{1}{2} U_i\right)} \tag{2.51}$$

for the BEP. It should be mentioned that the diversity order is given by

$$G_{\mathrm{d}} = \sum_{i=1}^{L} \min_{1\leq j\leq 4} \left\{\mu_{i,1}\alpha_{i,1}, \mu_{i,2}\alpha_{i,2}, z_{i,1}^2, z_{i,2}^2\right\}. \tag{2.52}$$

2.6 RESULTS

Theoretical curves as a function of the average SNR $\bar{\gamma}$ are shown in Fig. 2.1, corroborated by Monte-Carlo simulations, under different values of the parameter z in order to characterize scenarios with weak, moderate, and heavy pointing errors. The simulations consider the Fox H-function implementation available in [50]. In addition, $A_0 = 0.8$ and without loss of generality, $h_{\mathrm{l}} = 1$. The adherence between the theoretical and simulated curves is perceived in all cases. Also, the asymptotic curves follow the analytical ones at high SNR.

The SEP is evaluated in Fig. 2.1(a), with $\alpha = 3.5$, $m = 5$, and $\mu = 2.1$, for BPSK and QPSK modulation schemes. The asymptotic curves are plotted from (2.22). As z increases, it is noted that the SEP decreases since the pointing error condition is improving. For $\bar{\gamma} = 10$ dB, a difference in terms of SEP of approximately two orders of magnitude is perceived when comparing the curves for the case where the BPSK scheme is adopted, with weak ($z = 6.5$) and heavy ($z = 0.6$) pointing error scenarios. For z fixed, the SEP is better for the BPSK scheme than the one for QPSK, as the receiver is less likely to make errors in the decision process.

Fig. 2.1(b) presents OP curves under different values of α, for $\mu = 2.7$, $m = 1.3$ and $\gamma_{\text{th}} = 5$ dB. Asymptotic curves are plotted with (2.21). For $\alpha = 2$, the Fisher-Snedecor case is provided as a benchmark. As the parameter α increases, the OP improves for a given z value, since the higher the values of α are, the more deterministic the channel is and, therefore, the less vulnerable to variation the channel is [51]. Then, the increase of the parameter α diminishes the OP values. The following insight is also perceived in Fig. 2.1(b): for the strong pointing errors case, the increase in the value of α has almost no impact on the OP. Capacity and asymptotic capacity curves as a function of SNR are plotted in Fig. 2.1(c), under different m values, with $\alpha = 2.2$ and $\mu = 2.1$. In the analysis, $m = 3.1$ and $m = 10.5$ denote moderate and weak shadowing, respectively. Lower capacity values are obtained for $z = 0.6$, corresponding to a scenario with heavy pointing errors. Furthermore, smaller capacity values are also obtained for weak, moderate, or heavy pointing errors for $m = 3.1$.

Fig. 2.2 presents SEP curves as a function of average SNR $\bar{\gamma}$, considering the BPSK modulation scheme, $z = 3$, $m = \{2.5, \infty\}$, $\alpha = \{2, 6.5\}$ and $\mu = \{1, 1.7\}$. In the model, the α-μ with misalignment is obtained when $m \to \infty$. In turn, for $\alpha = 2$, the Fisher-Snedecor $\mathcal{F}$ distribution with pointing errors is achieved. For $\mu = 1$, the shadowed Weibull fading model, also with the mentioned effect, can be obtained as a particular case of the study proposed in this work. To the best of the authors' knowledge, results for the shadowed Weibull model with pointing errors have not been presented in the literature. In Fig. 2.2, it is evidenced that (i) for a fixed SNR, the SEP (symbol error probability) increases as the parameter that characterizes the shadowing (m) effect and/or the parameter that models the fading intensity decreases and (ii) the impact of the m and μ on the SEP is smaller as α increases.

Comparisons between the empirical and theoretical PDFs of the α-μ and α-$\mathcal{F}$ distributions are performed in Fig. 2.3. The empirical data were extracted from [16, Fig. 2(c)] using the WebPlotDigitizer tool [52], and the parameters of the theoretical PDFs were estimated using the `lsqcurvefit` function available in MATLAB. For the α-μ distribution, it should be mentioned that the estimated parameters are the same as found in [16, Table 5, TX4]. It is noted in Fig. 2.3 that the α-$\mathcal{F}$ model presents practically the same adherence as the α-μ distribution since the measured data did not consider shadowing. For this scenario, the α-$\mathcal{F}$ is slightly better than α-μ distribution in terms of MSE and has a large m value, which is expected in a non-

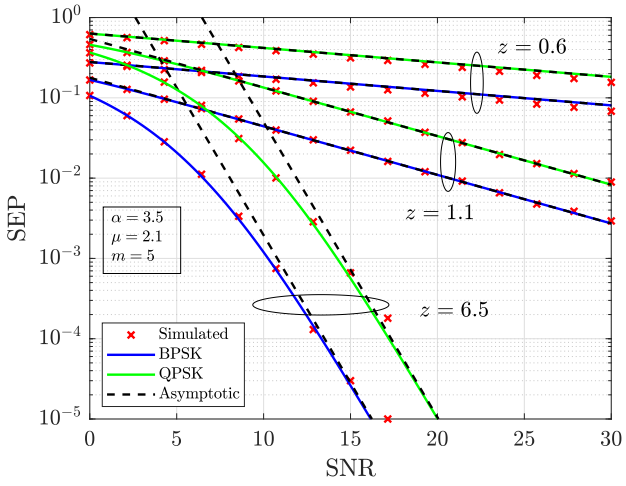

(a)

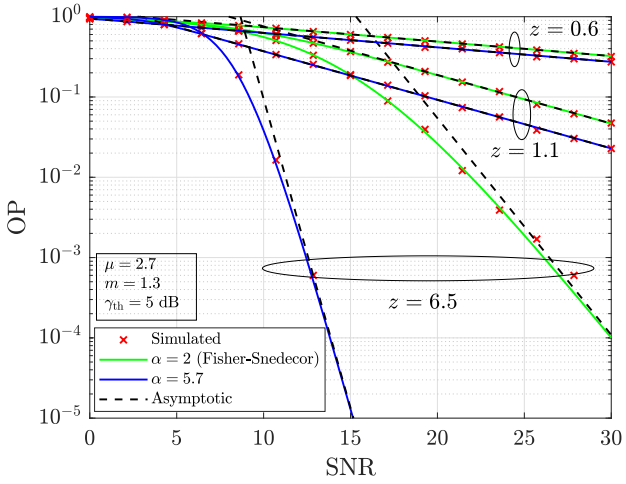

(b)

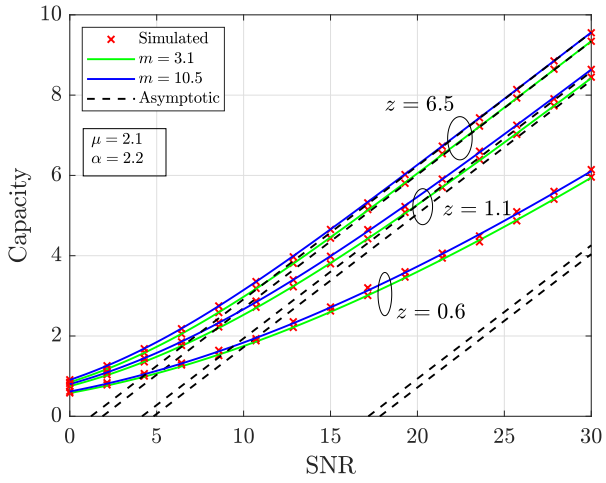

(c)

Figure 2.1. (a) SEP, (b) OP, and (c) capacity curves as a function of SNR $\bar{\gamma}$, considering weak, moderate, and heavy pointing errors.

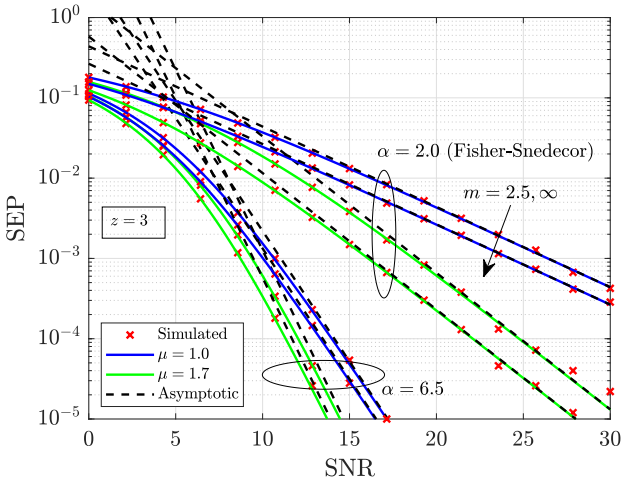

Figure 2.2. SEP curves as a function of SNR $\bar{\gamma}$, considering the BPSK modulation.

shadowing scenario. This supports the mathematical framework developed and the model itself. For the case in which shadowing can be considered, it is expected that the α-$\mathcal{F}$ distribution presents a better adherence than the α-μ since the mentioned distribution has a higher degree of freedom. This indicates the promising potential of employing the α-$\mathcal{F}$ distribution to model THz channels.

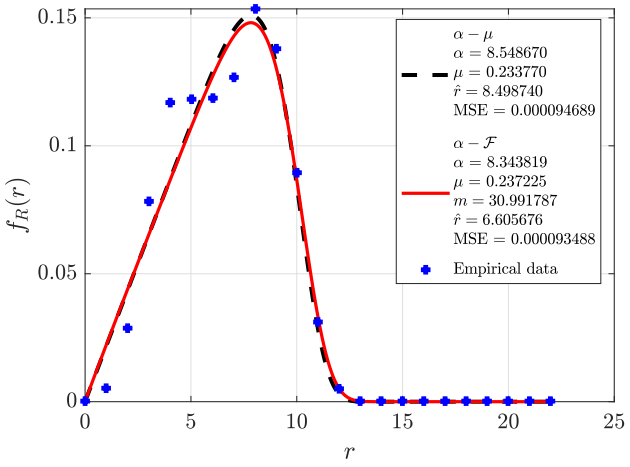

Figure 2.3. Comparisons between the empirical and the theoretical PDFs.

The OP and the BEP curves are presented in Figs. 2.4(a) and (b), respectively, under RIS-assisted scenarios considering α-$\mathcal{F}$ fading with pointing errors. In the study, independent and non-identically distributed variates are adopted. In Fig. 2.4(a), $\alpha_{i,1} = 1.5$, $\alpha_{i,2} = 2.3$, $\mu_{i,1} = \mu_{i,2} = 2.0$, $m_{i,1} = 3.0$, $m_{i,2} = 4.0$ and $\gamma_{\text{th}} = 5$ dB. In Fig. 2.4(b), $\alpha_{i,1} = 1.5$, $\alpha_{i,2} = 2.3$, $\mu_{i,1} = 2.5$, $\mu_{i,2} = 3.5$, $m_{i,1} = 4.0$, $m_{i,2} = 5.0$ and $\rho = 1$. The curves in Fig. 2.4 are shown as a

function of SNR for different numbers of the RIS elements under strong pointing errors. Curves concerning the non-pointing error case are included as benchmark. Asymptotic curves are also plotted with (2.45) and (2.46). In Fig. 2.4, the impact of the RIS elements on the metrics performance is evidenced. From the results, it is noted that the RIS improves the OP and BEP performance, consonant with (2.52). In fact, as L increases, the OP and BEP values obtained are lower. Furthermore, as evidenced in (2.52), it should be mentioned that the diversity gain depends on the fading and pointing errors parameters and, thus, note that the slope of the curves change according to the mentioned parameters.

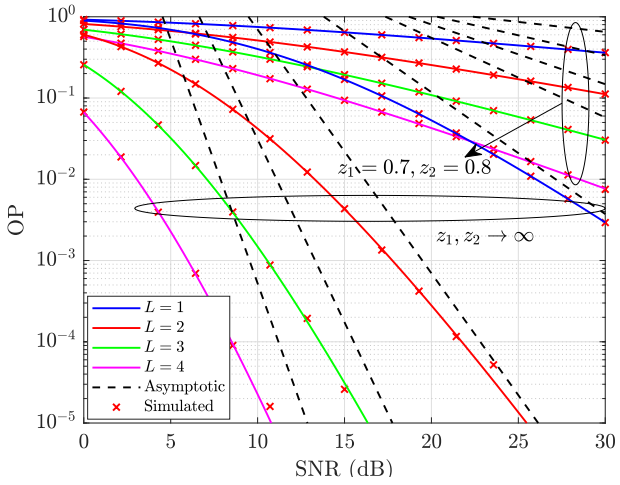

(a)

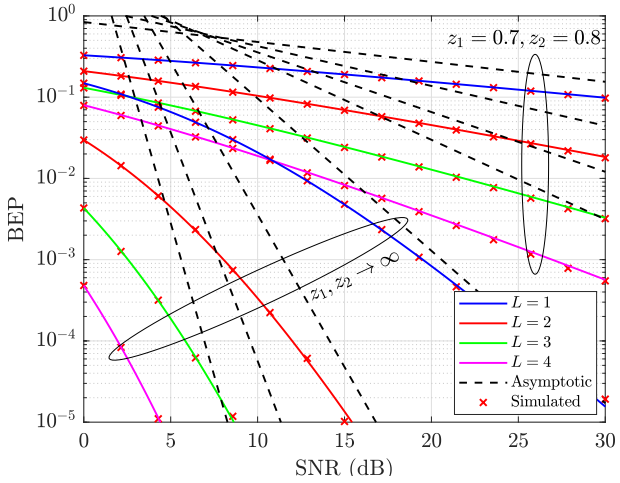

(b)

Figure 2.4. (a) OP and (b) BEP curves as a function of SNR $\bar{\gamma}$, under RIS-assisted scenarios, considering α-$\mathcal{F}$ fading with pointing errors.

CHAPTER 3

CASCADED AND SUM OF CASCADED OVER α-$\mathcal{F}$ FADING CHANNELS WITH POINTING ERROR IMPAIRMENT

Outline

In this chapter, the cascaded and the sum of cascaded α-$\mathcal{F}$ fading distribution with pointing errors is studied for the first time. All expressions derived in this work are new and generalist, written in terms of the single or multivariate Fox H-function [39]. The aforementioned expressions can be applied in different scenarios, including THz, RIS-assisted communications, multi-hop amplify and forward non-regenerative relaying systems, MIMO keyhole, or single-hop multiple-input single-output (MISO) systems, for example.

3.1 CASCADED α-$\mathcal{F}$ FADING WITH POINTING ERRORS CHANNELS

3.1.1 Cascaded System Model

The cascaded fading coefficient can be written as $H = H_1 H_2 \cdots H_N$, whose $H_j = h_{\mathrm{l}_j} H_{\mathrm{f}_j} H_{\mathrm{p}_j}$, $j = 1,2,\ldots,N$. The H_j PDF is given by

$$f_{H_j}(h_j) = \frac{\mathrm{H}_{2,2}^{2,1}\left[\Psi_j \left(\frac{h_j}{\hat{r}_j h_{\mathrm{l}_j} A_{0j}}\right)^{\alpha_j} \;\middle|\; \begin{matrix}(1-m_j,1),(z_j^2/\alpha_j+1,1)\\(\mu_j,1),(z_j^2/\alpha_j,1)\end{matrix}\right]}{h_j \Gamma(\mu_j)\Gamma(m_j)/z_j^2}, \tag{3.1}$$

where H_j is the j-th envelope fading channel characterized by the α-$\mathcal{F}$ composite distribution with pointing errors for each THz link, $\Psi_j = \mu_j/(m_j-1)$, $\hat{r}_j = \sqrt[\alpha_j]{\mathbb{E}[H_{\mathrm{f}_j}^{\alpha_j}]}$ is the α-root mean value, α_j characterizes the non-linearity of the propagation medium, μ_j represents the number of multipath clusters, m_j is the shadowing parameter, H[·] denotes the Fox H-function, A_{0j} is the fraction of the collected power, and z_j is the ratio between the equivalent beam radius at the receiver and the pointing error displacement standard deviation. For $z_j \to \infty$, it should be mentioned that the case of the non-pointing error is assumed.

It is assumed a THz link model with highly-directional transmit and receive antennas to ensure reliable energy transmission. In this model, H_{f_j} denotes the composite fading channel, H_{p_j} represents the misalignment component, and $h_{\mathrm{l}_j} = h_{\mathrm{fl}_j} h_{\mathrm{al}_j}$ is the deterministic path loss that is constant for a given weather condition and link distance. The parameter h_{fl_j} models the propagation gain and is given by

$$h_{\mathrm{fl}_j} = \frac{c\sqrt{G_{\mathrm{t}_j} G_{\mathrm{r}_j}}}{4\pi f d_j}, \tag{3.2}$$

in which G_{t_j} and G_{r_j} are, respectively, the gains of the transmit- and receive-antenna, c is the speed of light, f is the operating frequency, and d_j is the distance of the j-th hop such that $\sum_{j=1}^{N} d_j$ is the total distance of the link. In addition, h_{al_j} characterizes the molecular absorption gain and is given by

$$h_{\mathrm{al}_j} = \exp\left(-\frac{1}{2}\kappa_j(f) d_j\right), \tag{3.3}$$

in which $\kappa_j(f)$ denotes the frequency-dependent absorption coefficient. More details about h_{l_j} can be found in [2]. Thus, the received signal considering a wireless multi-hop amplify-and-forward relaying link can be written as

$$Y = \underbrace{H_1 H_2 H_3 \cdots H_N}_{H} X + W, \tag{3.4}$$

where X is the transmitted signal and W is the additive white Gaussian noise with zero mean and variance σ_W^2. It is assumed that $H_1, H_2, \cdots, H_N$ are independent.

3.1.2 First Order Statistics

Proposition 3.1.1. *Let α_j, μ_j, $\bar{\gamma}_j$, z_j, A_{0_j}, h_{l_j}, s, $\gamma \in \mathbb{R}^+$, and $m_j > 1$, with $j = 1,2,\ldots,N$. The PDF, the CDF, and the MGF of the instantaneous SNR Γ, under cascaded α-$\mathcal{F}$ composite fading with pointing errors, are given, respectively, by*

$$f_\Gamma(\gamma) = \frac{\mathrm{H}_{2N,2N}^{2N,N}\left[\Xi\sqrt{\gamma}\,\middle|\, \begin{matrix} \mathcal{A}_1, \cdots, \mathcal{A}_N, \mathcal{B}_1, \cdots, \mathcal{B}_N \\ \mathcal{C}_1, \cdots, \mathcal{C}_N, \mathcal{D}_1, \cdots, \mathcal{D}_N \end{matrix}\right]}{2\gamma \prod_{j=1}^{N} \alpha_j \Gamma(\mu_j)\Gamma(m_j)/z_j^2}, \tag{3.5}$$

$$F_\Gamma(\gamma) = \frac{\mathrm{H}_{2N+1,2N+1}^{2N,N+1}\left[\Xi\sqrt{\gamma}\,\middle|\, \begin{matrix} (1,1), \mathcal{A}_1, \cdots, \mathcal{A}_N, \mathcal{B}_1, \cdots, \mathcal{B}_N \\ \mathcal{C}_1, \cdots, \mathcal{C}_N, \mathcal{D}_1, \cdots, \mathcal{D}_N, (0,1) \end{matrix}\right]}{\prod_{j=1}^{N} \alpha_j \Gamma(\mu_j)\Gamma(m_j)/z_j^2} \tag{3.6}$$

and

$$\mathrm{M}_{\Gamma}(s) = \frac{\mathrm{H}_{2N+1,2N}^{2N,N+1}\left[\frac{\Xi}{\sqrt{s}}\middle| \begin{matrix}\left(1,\frac{1}{2}\right),\mathcal{A}_1,\cdots,\mathcal{A}_N,\mathcal{B}_1,\cdots,\mathcal{B}_N\\ \mathcal{C}_1,\cdots,\mathcal{C}_N,\mathcal{D}_1,\cdots,\mathcal{D}_N\end{matrix}\right]}{2\prod_{j=1}^{N}\alpha_j\Gamma(\mu_j)\Gamma(m_j)/z_j^2}, \tag{3.7}$$

where $\mathcal{A}_j = (1-m_j,1/\alpha_j)$, $\mathcal{B}_j = \left(z_j^2/\alpha_j+1,1/\alpha_j\right)$, $\mathcal{C}_j = (\mu_j,1/\alpha_j)$, $\mathcal{D}_j = \left(z_j^2/\alpha_j,1/\alpha_j\right)$, *and* $\Xi = \prod_{j=1}^{N}\Psi_j^{\frac{1}{\alpha_j}} z_j/\sqrt{\bar{\gamma}_j\left(z_j^2+2\right)}$, *in which* $\bar{\gamma}_j$ *is the average SNR and* N *is the number of channels.*

Proof. Let $H = H_1H_2\cdots H_N$, where $f_{H_j}(h_j)$, with $j = 1,2,\ldots,N$, is given by (3.1). The Mellin transform of $f_{H_j}(h_j)$, denoted by $\mathcal{M}[f_{H_j}(h_j)]$, can be derived by using [39, Eq. (2.9)] and making the variable change $r = h_j^{\alpha_j}$. According to [46, Eq. (3.5)],

$$\mathcal{M}[f_H(h)] = \mathcal{M}[f_{H_1}(h_1)]\mathcal{M}[f_{H_2}(h_2)]\cdots\mathcal{M}[f_{H_N}(h_N)],$$

and the PDF of H can be deduced by using [46, Eq. (3.2)]. After simplifications,

$$f_H(h) = \frac{1}{h}\left[\prod_{j=1}^{N}\frac{z_j^2}{\alpha_j\Gamma\left(\mu_j\right)\Gamma\left(m_j\right)}\right]\mathrm{H}_{2N,2N}^{2N,N}\left[\prod_{j=1}^{N}\frac{\Psi_j^{1/\alpha_j}}{\hat{r}_j h_{l_j}A_{0_j}}\middle| \begin{matrix}\mathcal{A}_1,\cdots,\mathcal{A}_N,\mathcal{B}_1,\cdots,\mathcal{B}_N\\ \mathcal{C}_1,\cdots,\mathcal{C}_N,\mathcal{D}_1,\cdots,\mathcal{D}_N\end{matrix}\right] \tag{3.8}$$

is obtained with $\mathcal{A}_j = (1-m_j,1/\alpha_j)$, $\mathcal{B}_j = \left(z_j^2/\alpha_j+1,1/\alpha_j\right)$, $\mathcal{C}_j = (\mu_j,1/\alpha_j)$, and $\mathcal{D}_j = \left(z_j^2/\alpha_j,1/\alpha_j\right)$.

Making $\Gamma = H^2$, the PDF of the instantaneous SNR (3.5) can be obtained by using the fact that $f_{\Gamma}(\gamma) = f_H(\sqrt{\gamma})/(2\sqrt{\gamma})$. Integrating (3.5), knowing that $\int_0^{\gamma} x^{n-1}\mathrm{d}x = \gamma^n/n$ and $\Gamma(\gamma+1) = \gamma\Gamma(\gamma)$, (3.6) is obtained. The MGF of Γ in (3.7) is obtained by making the Laplace transform of (3.5) and proceeding with some simplifications. Hence, the proof is concluded. □

3.1.3 Performance Metrics

3.1.3.1 Bit Error Probability

The average BEP, P_{b}, can be evaluated as

$$P_{\mathrm{b}} = \frac{1}{\pi}\int_0^{\frac{\pi}{2}}\mathrm{M}_{\Gamma}\left(\frac{\rho}{\sin^2\phi}\right)\mathrm{d}\phi, \tag{3.9}$$

in which ρ depends on the modulation type assumed.

Substituting (3.7) into (3.9), making $x = \sin^2(\phi)$, using [28, id 06.18.07.0001.01], [28, id 06.18.02.0001.01], and performing some simplifications, it follows that

$$P_{\mathrm{b}} = \frac{\mathrm{H}_{2N+2,2N+1}^{2N,N+2}\left[\frac{\Xi}{\sqrt{\rho}}\middle|\begin{matrix}\left(1,\frac{1}{2}\right),\left(\frac{1}{2},\frac{1}{2}\right),\mathcal{A}_1,\cdots,\mathcal{A}_N,\mathcal{B}_1,\cdots,\mathcal{B}_N\\ \mathcal{C}_1,\cdots,\mathcal{C}_N,\mathcal{D}_1,\cdots,\mathcal{D}_N,\left(0,\frac{1}{2}\right)\end{matrix}\right]}{4\sqrt{\pi}\prod_{j=1}^{N}\alpha_j\Gamma(\mu_j)\Gamma(m_j)/z_j^2}. \tag{3.10}$$

3.1.3.2 Outage Probability

The OP, P_{out}, is defined as the point at which the SNR of the signal at the output of the receiver falls below the threshold γ_{th}, i.e. $P_{\mathrm{out}} \triangleq \mathrm{Prob}[\Gamma \leq \gamma_{\mathrm{th}}] = F_{\Gamma}(\gamma_{\mathrm{th}})$. Then,

$$P_{\mathrm{out}} = \frac{\mathrm{H}_{2N+1,2N+1}^{2N,N+1}\left[\Xi\sqrt{\gamma_{\mathrm{th}}}\middle|\begin{matrix}(1,1),\mathcal{A}_1,\cdots,\mathcal{A}_N,\mathcal{B}_1,\cdots,\mathcal{B}_N\\ \mathcal{C}_1,\cdots,\mathcal{C}_N,\mathcal{D}_1,\cdots,\mathcal{D}_N,(0,1)\end{matrix}\right]}{\prod_{j=1}^{N}\alpha_j\Gamma(\mu_j)\Gamma(m_j)/z_j^2} \tag{3.11}$$

is deduced.

3.1.3.3 Ergodic Channel Capacity

The ergodic channel capacity, in bit/s, is calculated as

$$C_{\mathrm{erg}} = \frac{1}{\ln(2)}\int_0^{\infty} f_{\Gamma}(\gamma)\ln(1+\gamma)\mathrm{d}\gamma. \tag{3.12}$$

Replacing (3.5) into (3.12) and using [28, 01.04.26.0003.01] and [40, Eq. (2.8.4)], the channel capacity can be written as

$$C_{\mathrm{erg}} = \frac{\mathrm{H}_{2N+2,2N+2}^{2N+2,N+1}\left[\Xi\middle|\begin{matrix}(0,\frac{1}{2}),\mathcal{A}_1,\cdots,\mathcal{A}_N,\mathcal{B}_1,\cdots,\mathcal{B}_N,(1,\frac{1}{2})\\ \mathcal{C}_1,\cdots,\mathcal{C}_N,\mathcal{D}_1,\cdots,\mathcal{D}_N,(0,\frac{1}{2}),(0,\frac{1}{2})\end{matrix}\right]}{2\ln(2)\prod_{j=1}^{N}\alpha_j\Gamma(\mu_j)\Gamma(m_j)/z_j^2}. \tag{3.13}$$

3.1.3.4 Average AUC

The average AUC, $\bar{A}$, is given by [53, Eq. (36)]

$$\bar{A} = \int_0^{\infty} A(\gamma) f_{\Gamma}(\gamma)\mathrm{d}\gamma, \tag{3.14}$$

in which $A(\gamma)$ denotes the instantaneous AUC [53, Eq. (35)] given by

$$A(\gamma) = 1 - \sum_{k=0}^{u-1}\sum_{l=0}^{k}\binom{k+u-1}{k-l}\frac{\gamma^l\exp\left(-\gamma/2\right)}{2^{k+l+u}l!}, \tag{3.15}$$

where u denotes the time-bandwidth product under the energy detection technique and $\binom{a}{b}$ is the binomial coefficient. Replacing (3.5) and (3.15) in (3.14), using the integral representation of the H-function, [37, Eq. (3.381.4)] and [39, Eq. (1.2)] in sequence, one obtains

$$\bar{A} = 1 - \sum_{k=0}^{u-1} \sum_{l=0}^{k} \binom{k+u-1}{k-l} \frac{1}{2^{k+u+1} l!} \frac{\mathrm{H}_{2N+1,2N}^{2N,N+1}\left[\sqrt{2}\Xi \middle| \begin{matrix} (1-l,1/2), \mathcal{A}_1, \cdots, \mathcal{A}_N, \mathcal{B}_1, \cdots, \mathcal{B}_N \\ \mathcal{C}_1, \cdots, \mathcal{C}_N, \mathcal{D}_1, \cdots, \mathcal{D}_N \end{matrix}\right]}{\prod_{j=1}^{N} \alpha_j \Gamma(\mu_j)\Gamma(m_j)/z_j^2}. \tag{3.16}$$

3.1.4 Asymptotic Analysis

3.1.4.1 Bit Error Probability and Outage Probability

Considering the approach presented in [49], it follows that the asymptotic BEP and OP can be written as

$$P_{\mathrm{b}}^{\infty} = \frac{1}{B_\beta} \left[\prod_{j=1}^{N} \frac{z_j^2}{\alpha_j \Gamma(\mu_j)\Gamma(m_j)}\right] \frac{\phi \Gamma\left(\frac{U}{2}\right) \Gamma\left(\frac{U+1}{2}\right) \left(\frac{\Xi}{\sqrt{\rho}}\right)^U}{4\sqrt{\pi}\Gamma\left(\frac{U}{2}+1\right)} \tag{3.17}$$

and

$$P_{\mathrm{out}}^{\infty} = \frac{1}{B_\beta} \left[\prod_{j=1}^{N} \frac{z_j^2}{\alpha_j \Gamma(\mu_j)\Gamma(m_j)}\right] \frac{\phi \Gamma(U) \left(\gamma_{\mathrm{th}}^{\frac{1}{2}} \Xi\right)^U}{\Gamma(1+U)}, \tag{3.18}$$

respectively, where $U = \min\{\mu_1\alpha_1, \cdots, \mu_N\alpha_N, z_1^2, \cdots, z_N^2\}$, $\beta = \arg\min U$, and ϕ is given by (3.19). It should be mentioned that B_β is the residual term in the Fox H-function considered by removing the respective Gamma function from the condition $\mu_j \neq \frac{U}{\alpha_j}$ or $z_j^2 \neq U$ in (3.19).

$$\phi = \frac{\prod\limits_{\substack{j=1 \\ \mu_j \neq \frac{U}{\alpha_j}}}^{N} \Gamma\left(\mu_j - \frac{U}{\alpha_j}\right) \prod\limits_{\substack{j=1 \\ z_j^2 \neq U}}^{N} \Gamma\left(\frac{z_j^2 - U}{\alpha_j}\right) \prod\limits_{j=1}^{N} \Gamma\left(m_j + \frac{U}{\alpha_j}\right)}{\prod\limits_{j=1}^{N} \Gamma\left(\frac{z_j^2}{\alpha_j} + 1 - \frac{U}{\alpha_j}\right)} \tag{3.19}$$

From (3.17) and (3.18), the diversity order of the considered system can be found as

$$G_{\mathrm{d}} = \min(\alpha_1\mu_1/2, \cdots, \alpha_N\mu_N/2, z_1^2/2, \cdots, z_N^2/2). \tag{3.20}$$

That is, the diversity order depends on the fading and pointing error parameters.

3.1.4.2 Ergodic Channel Capacity

The asymptotic ergodic capacity at high SNR values is given by [42]

$$C_{\text{erg}}^{\infty} = \log_2(\bar{\gamma}) + \log_2(e)\frac{\partial}{\partial n}\frac{\mathbb{E}[\gamma^n]}{\bar{\gamma}^n}\bigg|_{n=0}, \tag{3.21}$$

in which $\partial/\partial n$ is the first derivative operator and

$$\mathbb{E}[\gamma^n] = \frac{\prod_{j=1}^{N} z_j^2 \Gamma\left(\mu_j + \frac{2n}{\alpha_j}\right)\Gamma\left(\frac{z_j^2+2n}{\alpha_j}\right)\Gamma\left(m_j - \frac{2n}{\alpha_j}\right)}{\Xi^{2n}\prod_{j=1}^{N}\alpha_j\Gamma(\mu_j)\Gamma(m_j)\Gamma\left(\frac{z_j^2}{\alpha_j}+1+\frac{2n}{\alpha_j}\right)}. \tag{3.22}$$

Replacing (3.22) into (3.21) and proceeding with simplifications,

$$C_{\text{erg}}^{\infty} = \log_2\left(\frac{1}{\Xi^2}\right) + \log_2(e)\left[\sum_{j=1}^{N}\frac{2}{\alpha_j}\left(\psi(\mu_j) + \psi\left(\frac{z_j^2}{\alpha_j}\right) - \psi(m_j) - \psi\left(\frac{z_j^2}{\alpha_j}+1\right)\right)\right], \tag{3.23}$$

with $\psi(x) = \Gamma'(x)/\Gamma(x)$ denoting the digamma function [37, Eq. (8.36)].

3.1.4.3 AUC

The asymptotic AUC is given by

$$\bar{A}^{\infty} = 1 - \sum_{k=0}^{u-1}\sum_{l=0}^{k}\binom{k+u-1}{k-l}\frac{\phi\Gamma\left(l+\frac{U}{2}\right)}{2^{k+u+1}l!B_{\beta}}\frac{(\sqrt{2}\Xi)^U}{\prod_{j=1}^{N}\alpha_j\Gamma(\mu_j)\Gamma(m_j)/z_j^2}, \tag{3.24}$$

that is derived from (3.16) using the approach presented in [49].

3.2 SUM OF CASCADED α-$\mathcal{F}$ FADING WITH POINTING ERROR CHANNELS

3.2.1 System Model

Let S be the sum of products of N α-$\mathcal{F}$ RVs with pointing errors, i.e.,

$$S = \sum_{i=1}^{L} H_{i1}H_{i2}\cdots H_{iN} = \sum_{i=1}^{L}\prod_{j=1}^{N} H_{ij},\ L \geq 1,\ N \geq 1. \tag{3.25}$$

The received signal, under the aforementioned model, can be written as

$$Y = \underbrace{\sum_{i=1}^{L} H_{i1}H_{i2}\cdots H_{iN}}_{S} X + W. \tag{3.26}$$

3.2.2 First Order Statistics

Proposition 3.2.1. *Consider* α_{ij}, μ_{ij}, $\bar{\gamma}_{ij}$, z_{ij}, $A_{0_{ij}}$, $h_{l_{ij}}$, s, $\gamma \in \mathbb{R}^+$, *and* $m_{ij} > 1$, *with* $j = 1,2,\ldots,N$ *and* $i = 1,2,\ldots,L$. *The PDF, the CDF, and the MGF of the instantaneous SNR* Γ, *considering the sum of independent and non-identically distributed cascaded* α-$\mathcal{F}$ *RVs with pointing errors, are given by*

$$f_\Gamma(\gamma) = \frac{\gamma^{-1}}{2}\left[\prod_{i=1}^{L}\sum_{j=1}^{N}\frac{z_{ij}^2}{\alpha_{ij}\Gamma(\mu_{ij})\Gamma(m_{ij})}\right] \times \mathrm{H}_{0,1:[2N+1,2N]_{i=1:L}}^{0,0:[2N,N+1]_{i=1:L}}\left[\begin{array}{c|c|c} \Xi_1\gamma^{\frac{1}{2}} & - & [(1,1),\mathcal{A}_{i1},\cdots,\mathcal{A}_{iN},\mathcal{B}_{i1},\cdots,\mathcal{B}_{iN}]_{i=1:L} \\ \vdots & (1,\{1\}_{i=1:L}) & [\mathcal{C}_{i1},\cdots,\mathcal{C}_{iN},\mathcal{D}_{i1},\cdots,\mathcal{D}_{iN}]_{i=1:L} \\ \Xi_L\gamma^{\frac{1}{2}} & & \end{array}\right], \quad (3.27)$$

$$F_\Gamma(\gamma) = \frac{1}{2}\left[\prod_{i=1}^{L}\sum_{j=1}^{N}\frac{z_{ij}^2}{\alpha_{ij}\Gamma(\mu_{ij})\Gamma(m_{ij})}\right] \times \mathrm{H}_{1,2:[2N+1,2N]_{i=1:L}}^{0,1:[2N,N+1]_{i=1:L}}\left[\begin{array}{c|c|c} \Xi_1\gamma^{\frac{1}{2}} & \left(1,\left\{\frac{1}{2}\right\}_{i=1:L}\right) & [(1,1),\mathcal{A}_{i1},\cdots,\mathcal{A}_{iN},\mathcal{B}_{i1},\cdots,\mathcal{B}_{iN}]_{i=1:L} \\ \vdots & (1,\{1\}_{i=1:L}),\left(0,\left\{\frac{1}{2}\right\}_{i=1:L}\right) & [\mathcal{C}_{i1},\cdots,\mathcal{C}_{iN},\mathcal{D}_{i1},\cdots,\mathcal{D}_{iN}]_{i=1:L} \\ \Xi_L\gamma^{\frac{1}{2}} & & \end{array}\right] \quad (3.28)$$

and

$$\mathrm{M}_\Gamma(s) = \frac{1}{2}\left[\prod_{i=1}^{L}\sum_{j=1}^{N}\frac{z_{ij}^2}{\alpha_{ij}\Gamma(\mu_{ij})\Gamma(m_{ij})}\right] \times \mathrm{H}_{1,1:[2N+1,2N]_{i=1:L}}^{0,1:[2N,N+1]_{i=1:L}}\left[\begin{array}{c|c|c} \Xi_1 s^{-\frac{1}{2}} & \left(1,\left\{\frac{1}{2}\right\}_{i=1:L}\right) & [(1,1),\mathcal{A}_{i1},\cdots,\mathcal{A}_{iN},\mathcal{B}_{i1},\cdots,\mathcal{B}_{iN}]_{i=1:L} \\ \vdots & (1,\{1\}_{i=1:L}) & [\mathcal{C}_{i1},\cdots,\mathcal{C}_{iN},\mathcal{D}_{i1},\cdots,\mathcal{D}_{iN}]_{i=1:L} \\ \Xi_L s^{-\frac{1}{2}} & & \end{array}\right], \quad (3.29)$$

respectively, where $\mathrm{H}[\cdot|\cdot|\cdot]$ *is the multivariate Fox H-function [39].*

Proof. Let be $S = Z_1 + Z_2 + \cdots + Z_L$, in which $f_{Z_i}(z)$ is given by (3.8). The MGF of S is given by $\mathrm{M}_S(s) = \mathrm{M}_{Z_1}(s)\mathrm{M}_{Z_2}(s)\cdots\mathrm{M}_{Z_L}(s)$, with each $\mathrm{M}_{Z_i}(s)$ being obtained by making the Laplace transform of $f_{Z_i}(z)$. Using [39, Eq. (A.13)], the product of the individual MGFs, $\mathrm{M}_S(s)$, can be derived in terms of the multivariate Fox H-function. Furthermore, using the Laplace inverse transform of $\mathrm{M}_S(s)$ and writing the multivariate Fox H-function in its integral form [39, Eq. A.1], the Laplace inverse transform integral can be internalized. Then, making the variable change $-t = sz$ and solving the inner integral, it is possible to use the fact that

$\frac{1}{\Gamma(x)} = \frac{w}{2\pi}\int_C (-t)^{-x}e^{-t}\mathrm{d}t$ to write the envelope PDF $f_S(s)$ in terms of another multivariate Fox H-function. After simplifications,

$$f_S(s) = \frac{1}{s}\left[\prod_{i=1}^{L}\prod_{j=1}^{N}\frac{z_{ij}^2}{\alpha_{ij}\Gamma\left(\mu_{ij}\right)\Gamma\left(m_{ij}\right)}\right] \times \mathrm{H}_{0,1:[2N+1,2N]_{i=1:L}}^{0,0:[2N,N+1]_{i=1:L}}\left[\begin{array}{c|c|c} \Omega_1 s & - & [(1,1),\mathcal{A}_{i1},\cdots,\mathcal{A}_{iN},\mathcal{B}_{i1},\cdots,\mathcal{B}_{iN}]_{i=1:L} \\ \vdots & (1,\{1\}_{i=1:L}) & [\mathcal{C}_{i1},\cdots,\mathcal{C}_{iN},\mathcal{D}_{i1},\cdots,\mathcal{D}_{iN}]_{i=1:L} \\ \Omega_L s & & \end{array}\right] \tag{3.30}$$

is deduced with $\Omega_i = \prod_{j=1}^{N}\Psi_{ij}^{1/\alpha_{ij}}/(\hat{r_{ij}}h_{l_{ij}}A_{0_{ij}})$ and $\Psi_{ij} = \mu_{ij}/(m_{ij}-1)$.

The PDF of the instantaneous SNR $\Gamma = S^2$ can be deduced by making $f_\Gamma(\gamma) = f_S(\sqrt{\gamma})/(2\sqrt{\gamma})$, which results in (3.27). By integrating (3.27) and by using similar steps presented in Appendix A, the CDF in (3.28) is obtained. The MGF of Γ shown in (3.29) is obtained by making the Laplace transform of (3.27) with some algebraic manipulations. Hence, the proof is concluded. □

3.2.3 Performance Metrics

3.2.3.1 Outage Probability

The OP is given by (3.31).

$$P_{\mathrm{out}} = \frac{1}{2}\left[\prod_{i=1}^{L}\prod_{j=1}^{N}\frac{z_{ij}^2}{\alpha_{ij}\Gamma(\mu_{ij})\Gamma(m_{ij})}\right] \times \mathrm{H}_{1,2:[2N+1,2N]_{i=1:L}}^{0,1:[2N,N+1]_{i=1:L}}\left[\begin{array}{c|c|c} \Xi_1\gamma_{\mathrm{th}}^{\frac{1}{2}} & \left(1,\left\{\frac{1}{2}\right\}_{i=1:L}\right) & [(1,1),\mathcal{A}_{i1},\cdots,\mathcal{A}_{iN},\mathcal{B}_{i1},\cdots,\mathcal{B}_{iN}]_{i=1:L} \\ \vdots & \left(1,\{1\}_{i=1:L}\right),\left(0,\left\{\frac{1}{2}\right\}_{i=1:L}\right) & [\mathcal{C}_{i1},\cdots,\mathcal{C}_{iN},\mathcal{D}_{i1},\cdots,\mathcal{D}_{iN}]_{i=1:L} \\ \Xi_L\gamma_{\mathrm{th}}^{\frac{1}{2}} & & \end{array}\right]. \tag{3.31}$$

3.2.3.2 Asymptotic Outage Probability

Considering the approach presented in [49], it follows that the asymptotic OP can be written as

$$P_{\text{out}}^{\infty} = \frac{1}{2\prod_{i=1}^{L} B_{\beta_i}} \left[\prod_{i=1}^{L} \prod_{j=1}^{N} \frac{z_{ij}^2}{\alpha_{ij}\Gamma(\mu_{ij})\Gamma(m_{ij})} \right] \Psi(U_1, \cdots, U_L) \left[\prod_{i=1}^{L} \phi \left(\Xi_i \gamma_{\text{th}}^{1/2} \right)^{U_i} \Gamma(U_i) \right], \quad (3.32)$$

with $U_i = \min\{\mu_{i1}\alpha_{i1}, \cdots, \mu_{iN_i}\alpha_{iN_i}, z_{i1}^2, \cdots, z_{iN}^2\}$, $\beta_i = \arg\min U_i$,

$$\Psi(U_1, \cdots, U_L) = \frac{\Gamma\left(\sum_{i=1}^{L} \frac{U_i}{2}\right)}{\Gamma\left(\sum_{i=1}^{L} U_i\right) \Gamma\left(1 + \sum_{i=1}^{L} \frac{U_i}{2}\right)}, \quad (3.33)$$

and ϕ given by (3.35). Note that B_{β_i} is the residual term in the Fox H-function considered by removing the respective Gamma function from the condition $\mu_{ij} \neq \frac{U_i}{\alpha_{ij}}$ or $z_{ij}^2 \neq U_i$ in (3.35). From (3.32), the diversity order is

$$G_{\text{d}} = \sum_{i=1}^{L} \min(\alpha_{i1}\mu_{i1}/2, \cdots, \alpha_{iN}\mu_{iN}/2, z_{i1}^2/2, \cdots, z_{iN}^2/2), \quad (3.34)$$

that depends on the fading and pointing error parameters.

$$\phi = \frac{\prod\limits_{\substack{j=1 \\ \mu_{ij} \neq \frac{U_i}{\alpha_{ij}}}}^{N} \Gamma\left(\mu_{ij} - \frac{U_i}{\alpha_{ij}}\right) \prod\limits_{\substack{j=1 \\ z_{ij}^2 \neq U_i}}^{N} \Gamma\left(\frac{z_{ij}^2 - U_i}{\alpha_{ij}}\right) \prod\limits_{j=1}^{N} \Gamma\left(m_{ij} + \frac{U_i}{\alpha_{ij}}\right)}{\prod\limits_{j=1}^{N} \Gamma\left(\frac{z_{ij}^2}{\alpha_{ij}} + 1 - \frac{U_i}{\alpha_{ij}}\right)} \quad (3.35)$$

3.3 NUMERICAL RESULTS

In Fig. 3.1, the performance of a relaying ($N = 2$) THz wireless communication system is investigated. Theoretical OP curves, from (3.11), and their asymptotics, from (3.18), as a function of average SNR $\bar{\gamma} = \bar{\gamma}_1 = \bar{\gamma}_2$ are shown, considering strong ($z_1 = 0.7$ and $z_2 = 0.8$), moderate ($z_1 = 1$ and $z_2 = 1.1$), and weak ($z_1 = 1.5$ and $z_2 = 1.6$) pointing error scenarios. Curves without misalignment, i.e. under non-pointing errors, are also presented as benchmarks, obtained when $\{z_1, z_2\} \to \infty$. For comparison purposes, the OP performance of a single ($N = 1$) THz link is also presented. The correctness of the derived expressions is unequivocally confirmed by the excellent correspondence between the theoretical expressions and Monte-Carlo simulation curves. Fig. 3.1 shows that (i) for a fixed SNR, the OP increases as the parameter that characterizes the pointing error (z) decreases, and (ii) the impact of the z on the OP is smaller

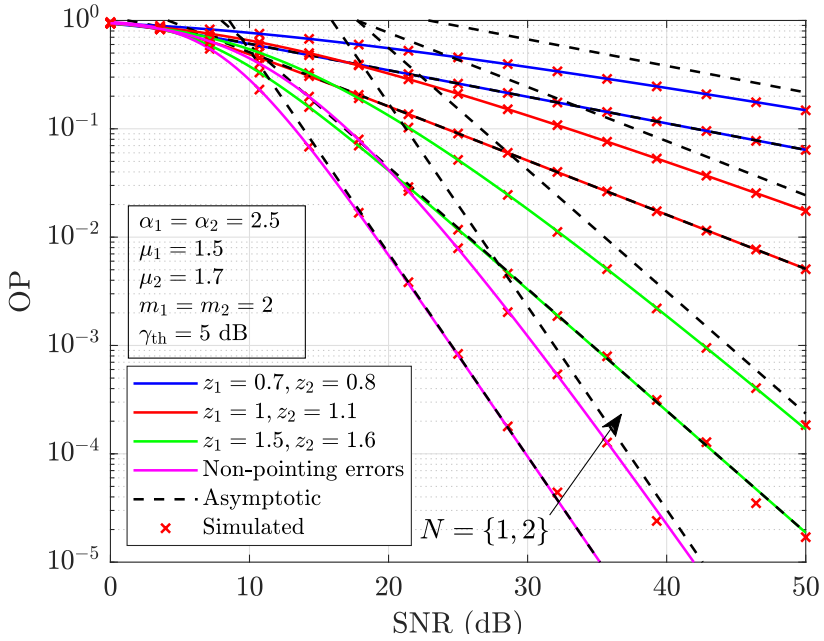

Figure 3.1. OP curves and their asymptotics as a function of SNR $\bar{\gamma}$, under different values of z_1, z_2 and number of channels N.

as N increases. Considering that the channel parameters are equal, the OP of the two-hop relaying THz system is higher than that of the single THz link. Furthermore, the results show that the asymptotic curves coincide with the analytical curves at high SNR values, again corroborating the correctness of the analytical results. As attested in theoretical findings, the diversity order, which is represented by the slope of asymptotic curves, depended only on the channel non-linearity and the pointing error parameter. For example, when the diversity gain equals $G_{\text{d}} = z_2^2/2 = 1.125$, $z_1 = 1.5$ and $z_2 = 1.6$, the curves for $N = 1$ and $N = 2$ have the same slope at high transmitted power.

BEP and asymptotic BEP curves as a function of average SNR $\bar{\gamma}$ are presented in Fig. 3.2, under strong, moderate, and weak pointing error conditions with $N = 2$. In all cases, for $\mu = \mu_1 = \mu_2 = 1$, the cascaded shadowed Weibull fading model with pointing errors is obtained as a particular case of the study proposed in this work. To the best of the author knowledge, results for the cascaded shadowed Weibull model with the aforementioned effect have not been presented in the literature. The non-pointing errors (obtained when $\{z_1,z_2\} \to \infty$) and no-shadowing (obtained when $m_1 = m_2 = m \to \infty$) cases are included in Figs. 3.2(a) and 3.2(b) as benchmarks, respectively. In Fig. 3.2(b), the purpose is to provide evidence of the impact of parameter m in the system performance. It can be seen in both figures that the performance

degrades as $\{z_1,z_2\}$ decreases. Furthermore, as shown in Fig. 3.2(b) for lower values of $\{z_1,z_2\}$, almost no impact has the shadowing intensity m in the BEP curves. In addition, the asymptotic curves have the same slope regardless of the value of m.

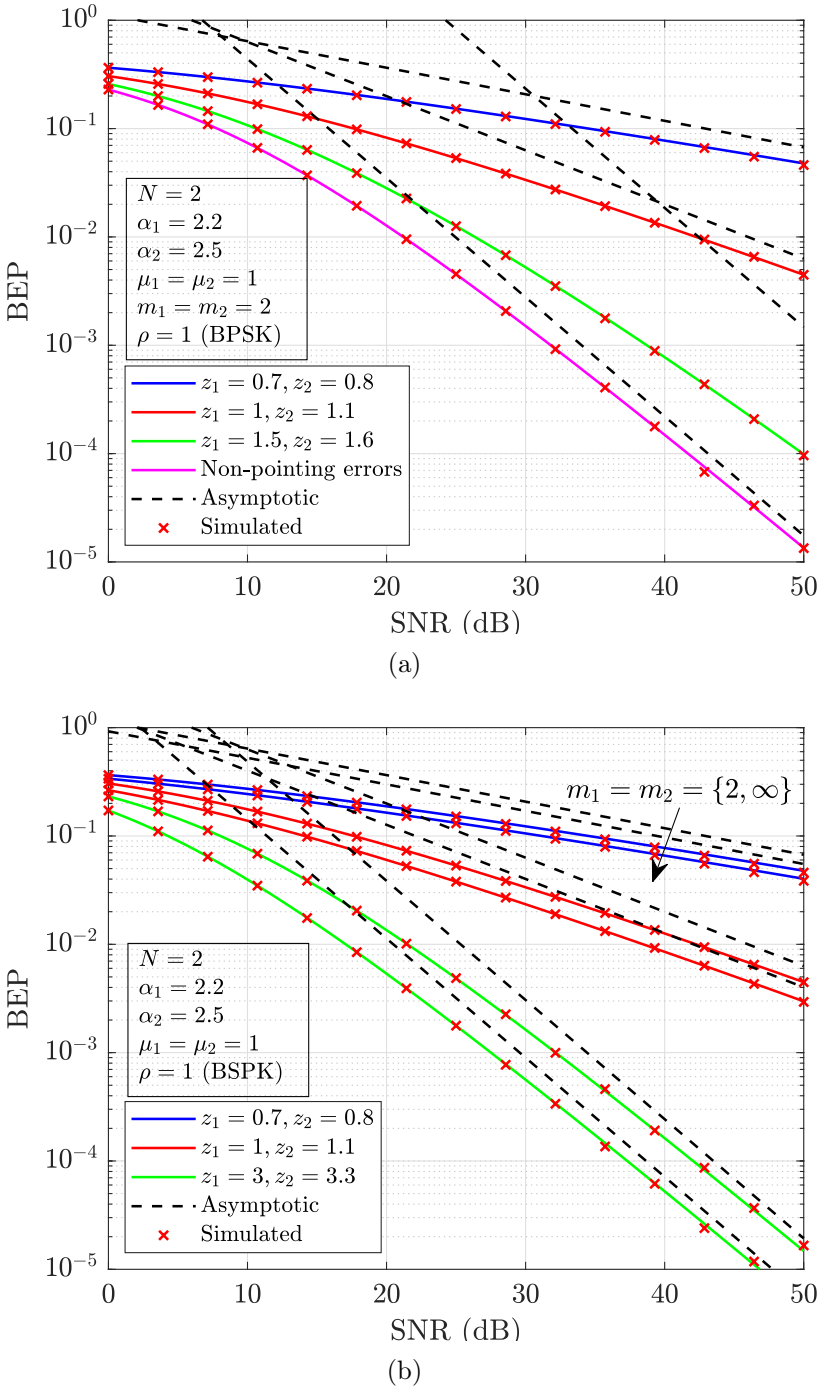

Figure 3.2. BEP and asymptotic BEP curves as a function of SNR $\bar{\gamma}$, under different values of (a) z; (b) m and z.

The performance of amplify-and-forward relaying THz systems in terms of the channel capacity is investigated in Fig. 3.3, for different values of $\alpha_1 = \alpha_2 = \alpha$ and pointing error

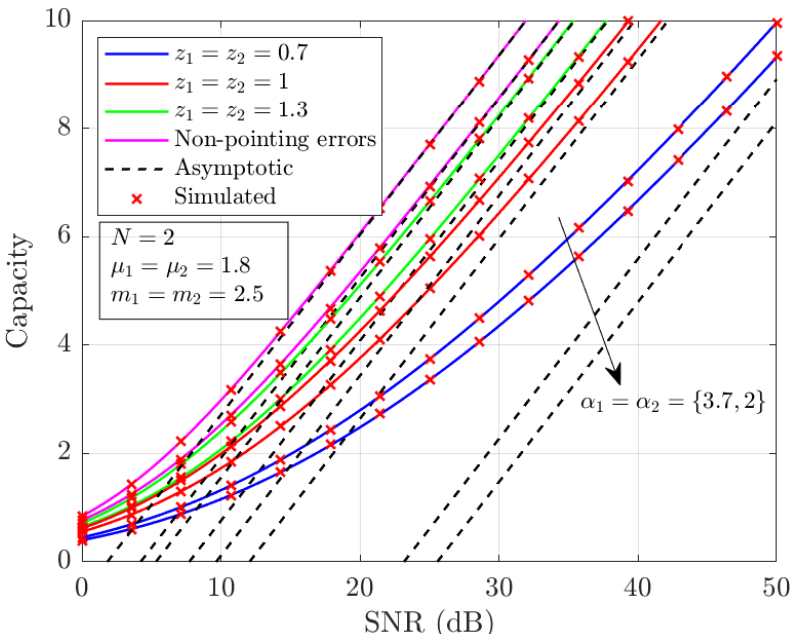

Figure 3.3. Channel capacity and asymptotic channel capacity curves as a function of SNR $\bar{\gamma}$ for different α and pointing error conditions.

conditions. The capacity improves as α and/or $z_1 = z_2$ increases since lower is the effect of the non-linearity and pointing errors in the system. Note that the best capacity curves are for the case in which non-pointing errors are considered. For $\alpha = 2$, the channel capacity corresponding to the cascaded Fisher-Snedecor $\mathcal{F}$ with pointing errors is presented as a benchmark.

AUC and asymptotic AUC curves are presented in Fig. 3.4, under different number of channels and considering particular cases of the study. It should be mentioned that the AUC metric assumes values between 0.5 and 1 and is used to evaluate the performance of the energy detection schemes. In Fig. 3.4, AUC curves for the Fisher Snedecor $\mathcal{F}$ and Weibull-$\mathcal{F}$ with pointing errors channels are presented. The mentioned cases are not analyzed in the literature, according to the best authors' knowledge. As the SNR increases, the detection performance gets better. It is noted in Fig. 3.4 that the energy detector performance depends on the fading parameters. As $\mu_1 = \mu_2 = \mu$ increases, the capability detection is improved. This occurs because of the advantages of the multipath effect. As benchmarks, AUC curves without pointing errors are also presented.

OP and asymptotic OP curves are presented in Fig. 3.5, under RIS-assisted scenarios considering α-$\mathcal{F}$ fading with pointing errors, for different numbers of the elements L present in the RIS and $\{z_1, z_2\}$ values. In the study, the non-pointing error condition is also considered. It

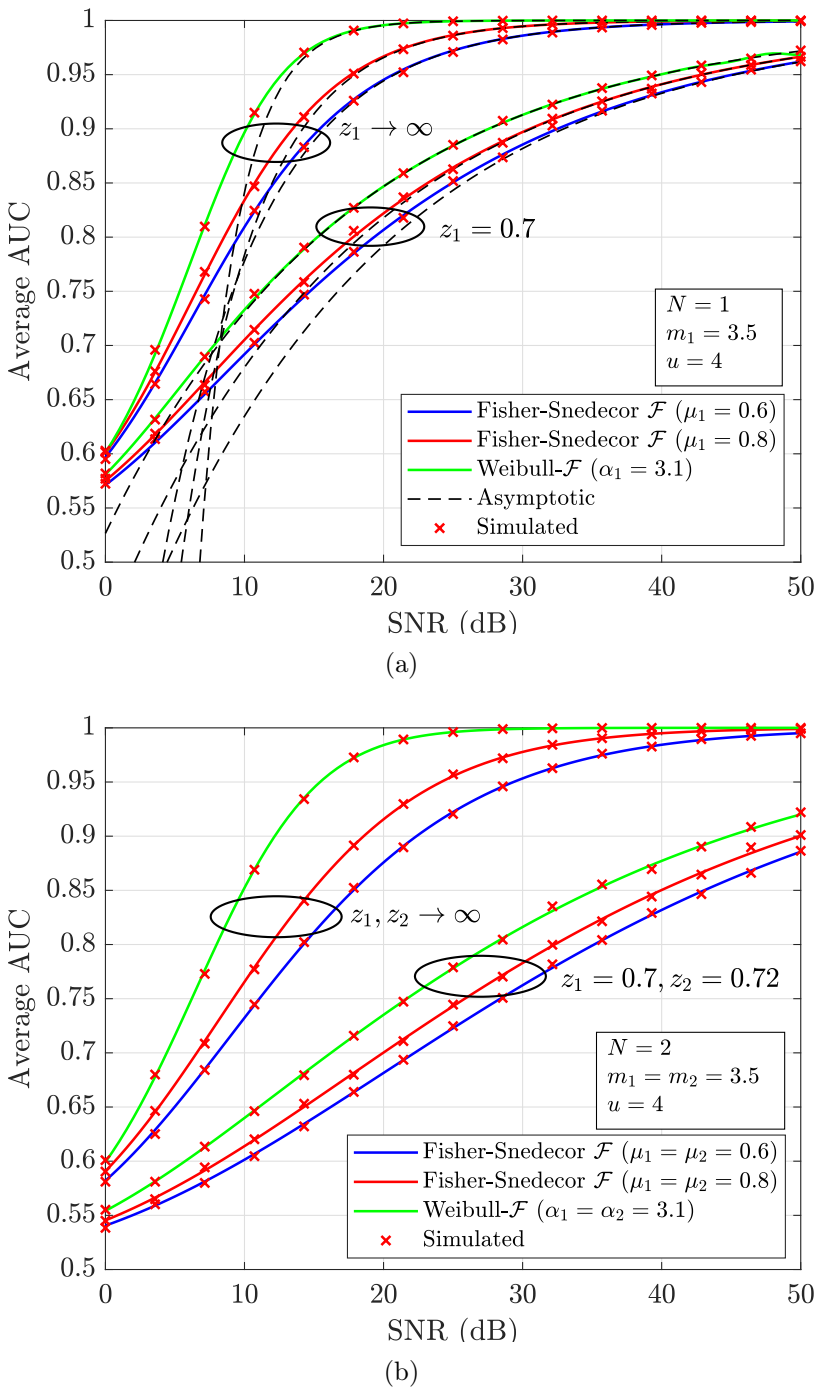

Figure 3.4. AUC and asymptotic AUC curves as a function of SNR $\bar{\gamma}$ for different fading models and number and channels.

should be mentioned that the scenario analyzed in this case corresponds to the sum of the product of two random variables. Note from Fig. 3.5 that the RIS improves the OP performance. In fact, as L increases, the OP values are lower.

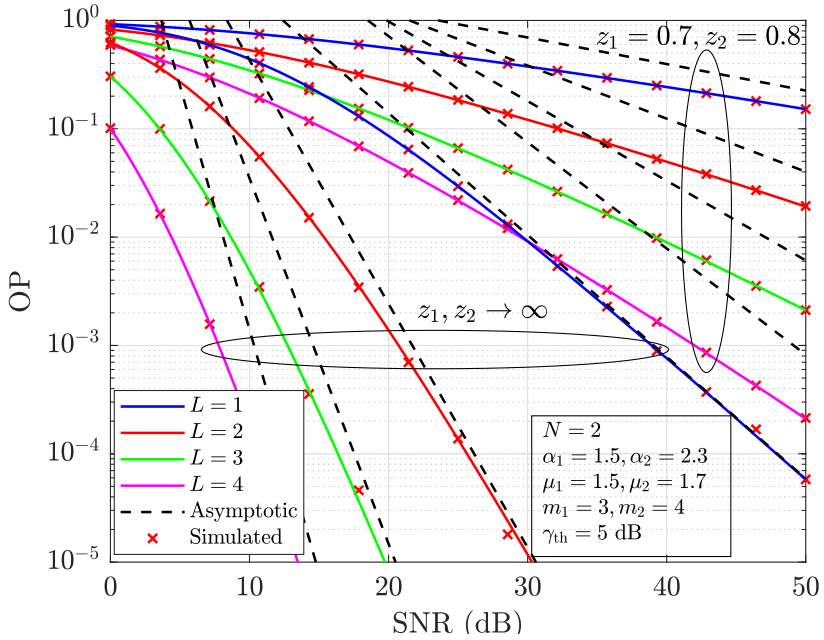

Figure 3.5. OP and asymptotic OP curves as a function of SNR $\bar{\gamma}$, under RIS-assisted scenarios considering α-$\mathcal{F}$ fading with and without pointing error condition.

CHAPTER 4

ON THE PERFORMANCE OF NOMA SYSTEMS OVER α-$\mathcal{F}$ FADING CHANNELS WITH POINTING ERROR IMPAIRMENT

Outline

This chapter presents the performance of NOMA under multipath, shadowing, non-linearity and pointing error impairment. Based on the existing literature, to the best of the author knowledge, none of the reports have studied the joint impact of the mentioned effects on the PEP performance of NOMA systems. Statistics are derived in this chapter, as well as closed-form and asymptotic expressions for the PEP under arbitrary NOMA users. The achievable theoretical diversity gains and the BER union bound are also analyzed. All the expressions presented in this work are unpublished.

4.1 SYSTEM MODEL

NOMA is a new and important technology used to improve the system spectral efficiency of the emergent and future communications wireless generations [26]. NOMA is a promising multiple access scheme in which many users are supported and multiplexed in the power domain, sharing the same time-frequency resources. In the before-mentioned technology, users adopt SIC to mitigate interference and enable proper signal detection.

The adopted downlink NOMA system is illustrated in Fig. 4.1 and consists of a single-antenna base station that transmits signals to L users using the same time-frequency resources. The transmitted signal s can be expressed as

$$s = \sum_{l=1}^{L} \sqrt{\beta_l \bar{\gamma}} x_l, \tag{4.1}$$

in which $\bar{\gamma}$ is the average transmitted SNR, x_l is the information symbol intended to the l-th user, $l = 1,2,\ldots,L$, and β_l is the corresponding power allocation coefficient, such that

$\sum_{l=1}^{L} \beta_l = 1$. The received signal at l-th user y_l is given by [19, Eq. (2)]

$$y_l = h_l s + w_l, \tag{4.2}$$

where h_l is the corresponding complex channel gain and w_l is the normalized complex additive white Gaussian noise with zero mean and unit variance. The system indexes users and allocates power according to the intensity of their channel gains. Therefore, the power allocation coefficients must satisfy $\beta_1 > \beta_2 > \cdots > \beta_L$ for channels ordered as $|h_1|^2 < |h_2|^2 < \cdots < |h_L|^2$.

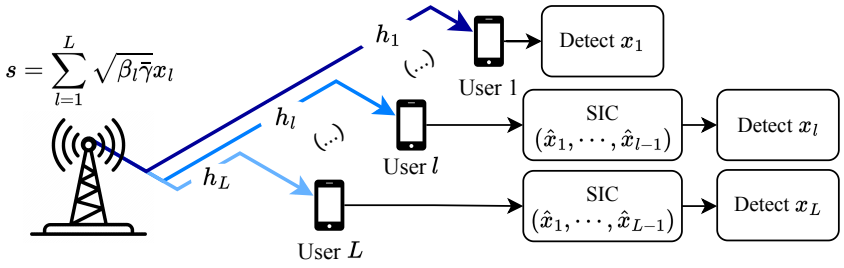

Figure 4.1. L-user NOMA system.

Since a given user receives a signal affected by the interference corresponding to the remaining $L-1$ users, the SIC process must be adopted to enable proper symbol detection. In this process, the l-th user detects and subtracts the symbols of the previous $l-1$ users. Without loss of generality, the l-th user detects his own symbol by applying a maximum likelihood detection based on

$$\hat{x}_l = \underset{\tilde{x} \in \mathcal{C}}{\operatorname{argmin}} \left| y'_l - \sqrt{\beta_l \bar{\gamma}} h_l \tilde{x} \right|^2, \tag{4.3}$$

in which $\mathcal{C}$ is an arbitrary signal constellation and y'_l is the output of the $(l-1)$-th SIC iteration, expressed by

$$y'_l = \left(\sqrt{\beta_l \bar{\gamma}} x_l + \underbrace{\sum_{j=1}^{l-1} \sqrt{\beta_j \bar{\gamma}} \delta_j}_{\text{SIC}} + \underbrace{\sum_{k=l+1}^{L} \sqrt{\beta_k \bar{\gamma}} x_k}_{\text{Interference}} \right) h_l + w_l. \tag{4.4}$$

In (4.4), $\delta_j = x_j - \hat{x}_j$, with $1 \leq j \leq l-1$. It can be seen from (4.4) that the first user ($l = 1$) does not perform SIC, resulting in $y'_l = y_l$. In contrast, the L-th user employs $L-1$ SIC iterations.

4.2 PDF OF THE l-TH USER

As aforementioned, the NOMA system indexes users in ascending order concerning channel intensity. Therefore, the instantaneous SNR is a user-dependent statistic. The PDF for the l-th user, $l = 1,2,\ldots,L$, is given by [20, Eq. (10)]

$$f_l(\gamma) = \frac{L! f_\gamma(\gamma)[F_\gamma(\gamma)]^{l-1}[1-F_\gamma(\gamma)]^{L-l}}{(l-1)!(L-l)!}. \tag{4.5}$$

Plugging (2.6) and (2.7) into (4.5) with simplifications, the PDF of the instantaneous SNR for the l-th user is written as

$$\begin{aligned} f_l(\gamma) = {} & \frac{L!\alpha^{1-l}}{2\gamma(l-1)!(L-l)!}\left(\frac{z^2}{\Gamma(\mu)\Gamma(m)}\right)^l \mathrm{G}_{2,2}^{2,1}\left[\Xi\middle|\begin{matrix}1-m, z^2/\alpha+1\\ \mu, z^2/\alpha\end{matrix}\right] \\ & \times\left[\mathrm{G}_{3,3}^{2,2}\left[\Xi\middle|\begin{matrix}1-m,1,z^2/\alpha+1\\ \mu, z^2/\alpha, 0\end{matrix}\right]\right]^{l-1} \\ & \times\left[1-\frac{z^2\alpha^{-1}}{\Gamma(\mu)\Gamma(m)}\mathrm{G}_{3,3}^{2,2}\left[\Xi\middle|\begin{matrix}1-m,1,z^2/\alpha+1\\ \mu, z^2/\alpha, 0\end{matrix}\right]\right]^{L-l}. \end{aligned} \tag{4.6}$$

In addition, using the binomial expansion to the term raised to the power $L-l$ and proceeding with some simplifications, (4.6) can be rewritten as

$$\begin{aligned} f_l(\gamma) = {} & \frac{L!\alpha}{2\gamma(l-1)!(L-l)!}\mathrm{G}_{2,2}^{2,1}\left[\Xi\middle|\begin{matrix}1-m, z^2/\alpha+1\\ \mu, z^2/\alpha\end{matrix}\right] \\ & \times\sum_{k=0}^{L-l}\binom{L-l}{k}(-1)^k\left(\frac{z^2}{\alpha\Gamma(\mu)\Gamma(m)}\right)^{l+k}\left[\mathrm{G}_{3,3}^{2,2}\left[\Xi\middle|\begin{matrix}1-m,1,z^2/\alpha+1\\ \mu, z^2/\alpha, 0\end{matrix}\right]\right]^{l+k-1}. \end{aligned} \tag{4.7}$$

From (4.6) or (4.7), for $\alpha = 2$, the Fisher-Snedecor model with pointing errors is obtained as a particular case of the study proposed in this work. To the best of the author knowledge, results for the Fisher-Snedecor model have not been presented in the literature concerning NOMA systems.

4.3 PERFORMANCE ANALYSIS FOR NOMA SYSTEMS UNDER α-$\mathcal{F}$ FADING WITH BEAM MISALIGNMENT

4.3.1 On the Exact PEP Analysis

The PEP for the l-th user, corresponding to a given transmitted and detected symbols pair $(x_l,\hat{x}_l)$, is expressed by [19]

$$\mathrm{PEP}_l = \int_0^\infty \mathrm{Q}(\Theta_l\sqrt{\gamma}) f_l(\gamma)\mathrm{d}\gamma, \tag{4.8}$$

in which $\mathrm{Q}(\cdot)$ is the Gaussian Q-function [37] and

$$\Theta_l = \sqrt{\frac{\beta_l \bar{\gamma}}{2}}|\delta_l| + \frac{2}{|\delta_l|}\sqrt{\frac{\bar{\gamma}}{2}}\Re\left\{\delta_l\left(\sum_{i=1}^{l-1}\sqrt{\beta_i}\delta_i^* + \sum_{j=l+1}^{L}\sqrt{\beta_j}x_j^*\right)\right\}, \tag{4.9}$$

with $\delta_l = x_l - \hat{x}_l$, $\Re\{\cdot\}$ representing the real part operator, and $(\cdot)^*$ denoting the complex conjugate.

Using the fact that [39]

$$\mathrm{Q}(\Theta_l\sqrt{\gamma}) = \frac{1}{2\sqrt{\pi}}\mathrm{H}_{1,2}^{2,0}\left[\frac{\Theta_l^2}{2}\gamma\middle|\begin{matrix}(1,1)\\(0,1),(\frac{1}{2},1)\end{matrix}\right], \tag{4.10}$$

writing each Meijer G-function in (4.7) in terms of the Mellin-Barnes integral and replacing the resulting expressions in (4.8), it is possible to write the PEP as

$$\begin{aligned}\mathrm{PEP}_l = {} & \frac{L!\alpha}{4\sqrt{\pi}(l-1)!(L-l)!}\sum_{k=0}^{L-l}\binom{L-l}{k}(-1)^k\left(\frac{z^2}{\alpha\Gamma(\mu)\Gamma(m)}\right)^{l+k}\frac{1}{(2\pi j)^{l+k}}\\ & \times\int_{\mathcal{L}_1}\cdots\int_{\mathcal{L}_{l+k}}\prod_{i=1}^{l+k}\phi_i(\tau_i)\left(\frac{\Psi z^\alpha}{(\bar{\gamma}(z^2+2))^{\alpha/2}}\right)^{-\tau_i}\\ & \times\underbrace{\int_0^\infty\gamma^{-1-\frac{\alpha}{2}\sum_{i=1}^{l+k}\tau_i}\mathrm{H}_{1,2}^{2,0}\left[\frac{\Theta_l^2}{2}\gamma\middle|\begin{matrix}(1,1)\\(0,1),(\frac{1}{2},1)\end{matrix}\right]\mathrm{d}\gamma}_{\mathcal{I}}\,\mathrm{d}\tau_1\cdots\mathrm{d}\tau_{l+k},\end{aligned} \tag{4.11}$$

with

$$\phi_i(\tau_i) = \frac{\Gamma(\mu+\tau_i)\Gamma(z^2/\alpha+\tau_i)\Gamma(m-\tau_i)\Gamma(-\tau_i)}{\Gamma(z^2/\alpha+1+\tau_i)\Gamma(1-\tau_i)} \tag{4.12}$$

for $1 \le i \le l+k-1$ and

$$\phi_i(\tau_i) = \frac{\Gamma(\mu+\tau_{k+l})\Gamma(z^2/\alpha+\tau_{k+l})\Gamma(m-\tau_{k+l})}{\Gamma(z^2/\alpha+1+\tau_{k+l})} \tag{4.13}$$

for $i = l+k$. Solving the inner integral $\mathcal{I}$ by means of [39, Eq. (2.8)] and using [39, Eq. (A.1)], it is possible to write the PEP in terms of the multivariate Fox H-function [39] as

$$\begin{aligned}\mathrm{PEP}_l = {} & \frac{L!\alpha}{4\sqrt{\pi}(l-1)!(L-l)!}\sum_{k=0}^{L-l}\binom{L-l}{k}(-1)^k\left(\frac{z^2}{\alpha\Gamma(\mu)\Gamma(m)}\right)^{l+k}\\ & \times\mathrm{H}_{2,1:2,2:[3,3]_{i=1:l+k-1}}^{0,2:2,1:[2,2]_{i=1:l+k-1}}\left[\begin{matrix}\Omega_1\\\vdots\\\Omega_{l+k}\end{matrix}\middle|\begin{matrix}\varepsilon_1,\varepsilon_2\\\varepsilon_3\end{matrix}\middle|\begin{matrix}(1-m,1),(\frac{z^2}{\alpha}+1,1)\\(\mu,1),(\frac{z^2}{\alpha},1)\end{matrix}\middle|\begin{matrix}\left[(1-m,1),(1,1),(\frac{z^2}{\alpha}+1,1)\right]_{i=1:l+k-1}\\\left[(\mu,1),(\frac{z^2}{\alpha},1),(0,1)\right]_{i=1:l+k-1}\end{matrix}\right]\end{aligned} \tag{4.14}$$

with

$$\Omega_i = \frac{\Psi(\sqrt{2}z)^\alpha}{(\Theta_l^2(z^2+2))^{\alpha/2}}, \tag{4.15}$$

$\varepsilon_1 = \left(1;\left\{\frac{\alpha}{2}\right\}_{i=1:k+l}\right)$, $\varepsilon_2 = \left(\frac{1}{2};\left\{\frac{\alpha}{2}\right\}_{i=1:k+l}\right)$, and $\varepsilon_3 = \left(0;\left\{\frac{\alpha}{2}\right\}_{i=1:k+l}\right)$.

4.3.2 On the Asymptotic PEP Analysis

The asymptotic PEP for the l-th user, derived following [49] and considering the dominant term, is given by

$$\mathrm{PEP}_l^{\infty} = \frac{L!\Gamma\left(\frac{1}{2}+\frac{\alpha\mu}{2}l\right)}{2l\sqrt{\pi}(l-1)!(L-l)!}\left[\frac{\Psi^{\mu}z^2\Gamma(m+\mu)}{\left(\frac{z^2}{\alpha}-\mu\right)\alpha\mu\Gamma(\mu)\Gamma(m)}\left(\frac{z\sqrt{2}}{\sqrt{\Theta_l^2(z^2+2)}}\right)^{\alpha\mu}\right]^l \tag{4.16}$$

for $\alpha\mu < z^2$ and by

$$\mathrm{PEP}_l^{\infty} = \frac{L!\Gamma\left(\frac{1}{2}+\frac{z^2}{2}l\right)}{2l\sqrt{\pi}(l-1)!(L-l)!}\left[\frac{\Psi^{\frac{z^2}{\alpha}}\Gamma(\mu-\frac{z^2}{\alpha})\Gamma(m+\frac{z^2}{\alpha})}{\Gamma(\mu)\Gamma(m)}\left(\frac{z\sqrt{2}}{\sqrt{\Theta_l^2(z^2+2)}}\right)^{z^2}\right]^l \tag{4.17}$$

for $\alpha\mu > z^2$.

4.3.3 Diversity Gain Analysis

The diversity gain for the l-th user, defined as the slope of the PEP, when the SNR tends to infinity, can be calculated as

$$\mathcal{G}_{\mathrm{d}} = \lim_{\bar{\gamma}\to\infty} -\frac{\log(\mathrm{PEP}_l)}{\log(\bar{\gamma})} = -\frac{\log(\mathrm{PEP}_l^{\infty})}{\log(\bar{\gamma})}. \tag{4.18}$$

Using (4.16) and (4.17) in (4.18), it follows that

$$\mathcal{G}_{\mathrm{d}} = \begin{cases} z^2 l, & \text{if } \alpha\mu > z^2, \\ \alpha\mu l, & \text{if } \alpha\mu < z^2. \end{cases} \tag{4.19}$$

4.3.4 BER Union Bound

Evaluating system performance by error rate using the union bound is an effective approach in cases where the derivation of an analytical expression is overly complex. The BER union bound can be written as a function of the individual PEPs as [19, Eq. (27)]

$$P_{\mathrm{b}} \leq \frac{1}{k}\sum_{x_l\in\mathcal{C}}\Pr(x_l)\sum_{\substack{\hat{x}_l\in\mathcal{C}\\ \hat{x}_l\neq x_l}} q(x_l,\hat{x}_l)\mathrm{PEP}_l, \tag{4.20}$$

in which k is the number of bits per symbol, $\Pr(x_l)$ is the probability of transmitting symbol x_l, $q(x_l,\hat{x}_l)$ is the number of bit errors when detecting $\hat{x}_l$ instead x_l, and PEP_l is the PEP conditioned to the symbol pair $(x_l,\hat{x}_l)$, expressed analytically by (4.14).

4.4 NUMERICAL RESULTS AND REMARKS

This section presents the analytical and numerical results related to the PEP expressions derived in this study. The diversity gain and the BER union bound are also evaluated. In addition, numerical results of Monte Carlo simulations are shown. By analyzing (4.8), one can observe that the PEP for a given transmitted and detected symbol pair $(x_l,\hat{x}_l)$ can be expressed as the expected value of $\mathrm{Q}(\Theta_l\sqrt{\gamma})$. The Monte Carlo simulations for the PEPs compute the sample mean of $\mathrm{Q}(\Theta_l\sqrt{\gamma})$, using the numerical inverse polynomial method to generate samples of γ to each user according to the PDF in (2.6). The samples are then ordered according to the user index to obtain the l-th user statistic as in (4.6). The average SNR $\bar{\gamma}$, the system parameters, and the iterations of the imperfect SICs are encapsulated in the term Θ_l. It should be noted that the PEP is dependent upon the chosen symbol pair $(x_l,\hat{x}_l)$. Without loss of generality, it is assumed as $x_l = -1-j$ and $\hat{x}_l = -1+j$ for any $l = 1,2,\ldots,L$, corresponding to symbols in the normalized quadrature phase shift keying constellation (QPSK). The following results consider $L = 3$ users and a power allocation such that $\beta_1 = 0.7$, $\beta_2 = 0.2$, and $\beta_3 = 0.1$. Different combinations of the α-$\mathcal{F}$ distribution parameters are exercised to assess the impact of the channel behavior.

Fig. 4.2 presents the exact and asymptotic curves for the PEPs of the $L = 3$ users as a function of the average SNR for fixed $\alpha = 3.5$, $\mu = 1.5$, and $m = 3$. Two contrasting scenarios are analyzed: one with a strong impact of the pointing error ($z = 0.7$) and another in the absence of pointing errors ($z \to \infty$). It can be observed that performance improves for users who perform more SIC steps, and the third user experiences the best PEP for a given average SNR. Furthermore, one can notice the strong impact of the pointing error on the PEPs. For example, the system affected by the pointing error requires an average SNR of approximately 19 dB to guarantee a PEP equal to 10^{-3} for the third user. In contrast, this user achieves the same PEP level with an average SNR of -1.6 dB in a scenario without pointing errors. It should be noted that the curves of the exact expressions correspond with excellent precision to the results of the numerical simulations, confirming the correctness of the derived expressions. In addition, the analytical curves tend to the limits established by the asymptotic expressions in a high SNR regime.

PEP curves as a function of z are presented in Fig. 4.3 for $\alpha = 2$ (Fisher-Snedecor) and

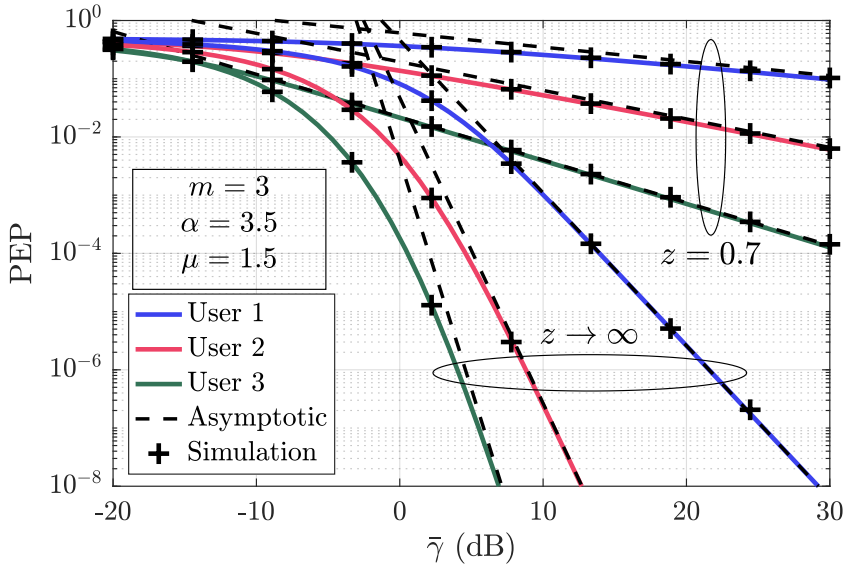

Figure 4.2. Analytical, asymptotic, and simulated PEPs as a function of the average SNR, considering different values for the parameter z.

$\alpha = 8$, fixed $m = \mu = 2$, and $\bar{\gamma} = 5$ dB. The results in Fig. 4.3 indicate that the impact of pointing errors on the PEP experienced by users vanishes for moderately high values of z. Specifically, at approximately $z = 5$, the pointing error no longer affects the PEP. Conversely, it is observed that the effect of channel nonlinearity, represented by a decrease in the α parameter, can significantly degrade system performance.

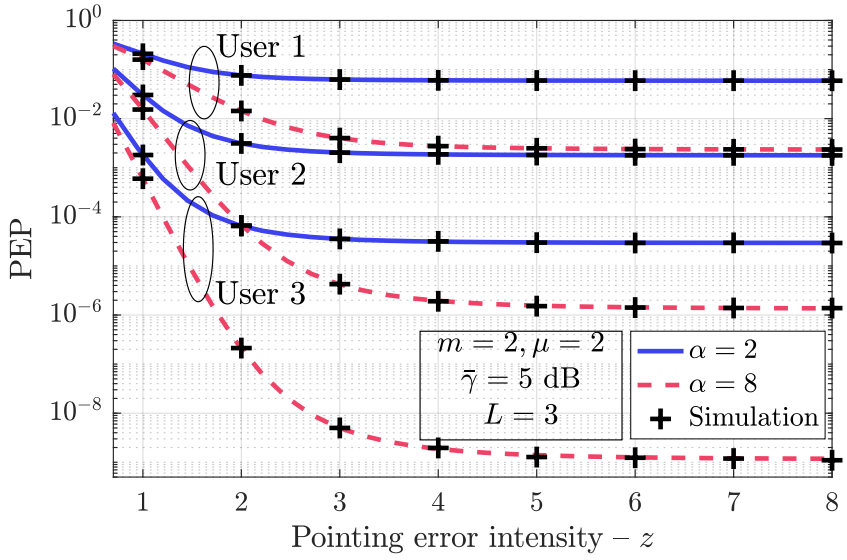

Figure 4.3. PEP curves as a function of z under different values of α.

An analysis of the diversity gain is presented in Fig. 4.4 under fixed values of $m = 3$, $\alpha = 2$, and $\mu = 2$. Two scenarios for the pointing error are evaluated, with $z = 2$ (left) and

$z = 3$ (right), corresponding to the cases in which $\alpha\mu > z^2$ and $\alpha\mu < z^2$, respectively. As expected, the numerical curves converge to the limit imposed by the diversity gain at high SNR, confirming the behavior proportional to the user index established in Section 4.3.3.

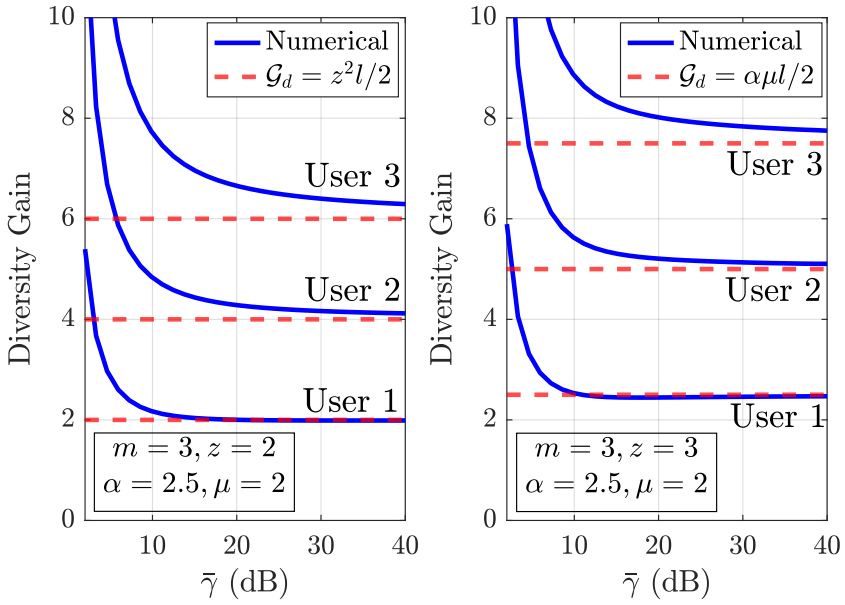

Figure 4.4. User diversity gains for $\alpha\mu > z^2$ (left) and $\alpha\mu < z^2$ (right).

Fig. 4.5 presents exact BER curves, generated by simulations, alongside the corresponding BER union bound, from (4.20), for a network with $L = 2$ users and fixed $\alpha = 3$ and $\mu = 2$. Two scenarios are examined: one with strong shadowing and pointing errors, characterized by parameters $z = 1$ and $m = 2$, and another without impact from these effects, where $z \to \infty$ and $m \to \infty$. The network configuration employs a power allocation scheme with $\beta_1 = 0.8$ and $\beta_2 = 0.2$, using equiprobable symbols from a binary phase shift keying (BPSK) constellation. It is crucial to note that deriving the union bounds from (4.20) requires considering all possible combinations of transmitted and detected symbols for all users, followed by calculating the average of these outcomes, given that the l-th user's PEP depend on different combinations of x_l and δ_j, with $j \in [1, l-1]$. In turn, the BER Monte Carlo simulations are performed reproducing the system structure as presented in Section 4.1.

From the results presented in Fig. 4.5, it can be noted that the union bound follows the same trend as the BER with a relatively low overestimation of the error rate, which indicates that this metric is a suitable approach to evaluate system performance. Additionally, it can be observed that, in the scenario without shadowing and pointing errors, there are SNR regimes in

which the second user does not outperform the first. Only when the SNR exceeds approximately 10 dB does the BER of the second user become better than that of the first. This behavior occurs because, for SIC to be effective, the second user requires a sufficiently high SNR to accurately detect the first user's symbol. If this condition is unmet, the additional SIC process can adversely affect higher-order users' performance. Additionally, severe fading significantly degrades system performance, increasing BER levels.

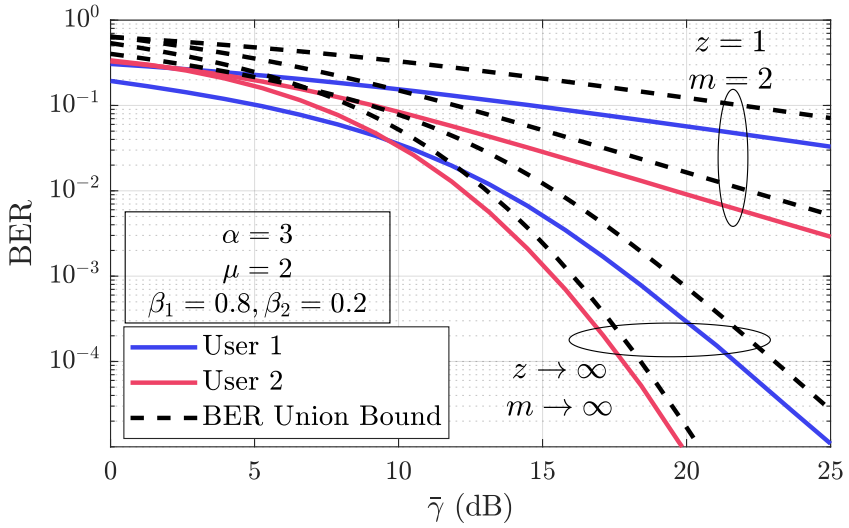

Figure 4.5. Simulated BER and BER union bound curves.

CHAPTER 5

CONCLUSIONS

This dissertation has advanced the knowledge of the α-$\mathcal{F}$ fading model by considering the pointing errors impairment. Important statistics, such as the PDFs and the CDFs, higher-order moments, and moment generating functions of the instantaneous SNR, were derived, as well as the outage probability, symbol error probability, and ergodic channel capacity metrics. Curves have been presented for the mentioned metrics and validated using Monte-Carlo simulations. A strong adherence between the theoretical and simulated curves has been noticed in all scenarios studied, which validates the analysis. In addition, an application of the α-$\mathcal{F}$ distribution with pointing errors has been performed in reconfigurable intelligent surfaces, multihop and NOMA wireless emerging systems, thus evidencing the usefulness of the model in practical scenarios.

As future works:

- The overall expressions have been written in terms of a single Fox H-function when dealing with the proposed cascaded of α-$\mathcal{F}$ RVs with pointing errors. However, when dealing with the sum of cascaded, over the application on the channel characterization of RIS systems, the mathematical complexity has led to intricate expressions. So far, if it is possible, a simpler expression has not been found under this comprehensive scenario. Based on some simplifications available elsewhere in the literature, there may be ways to find simpler expressions under not-so-restrictive assumptions. For instance, using discrete values for the number of multipath clusters, i.e., for the corresponding μ parameter, may simplify the expressions. However, this can be a trick task provided that even some already reported particular cases in the literature have been given in terms of the multivariate Fox H-function. But this requires further investigation.

- Assess the performance of a conventional wireless system jointly subject to short-term fading, long-term fading, path loss, non-linearity and mobility through analytical formulations.

BIBLIOGRAPHY

[1] C. Han, Y. Wang, Y. Li, Y. Chen, N. A. Abbasi, T. Kürner and A. F. Molisch, "Terahertz wireless channels: A holistic survey on measurement, modeling, and analysis," ArXiv, pp. 1-40, Jul. 2022. Cited on page 1.

[2] A. A. Boulogeorgos, E. N. Papasotiriou and A. Alexiou, "Analytical performance assessment of THz wireless systems," *IEEE Access*, vol. 7, pp. 11436-11453, Jan. 2019. Cited 5 times on pages 1, 2, 6, 7, and 23.

[3] M. T. Dabiri and M. Hasna, "Pointing error modeling of mmWave to THz high-directional antenna arrays," *IEEE Wirel. Commun. Lett.*, vol. 11, no. 11, pp. 2435-2439, Nov. 2022. Cited 2 times on pages 1 and 7.

[4] O. S. Badarneh, "Performance analysis of terahertz communications in random fog conditions with misalignment," *IEEE Wirel. Commun. Lett.*, vol. 11, no. 5, 962-966, May 2022. Cited on page 2.

[5] A. A. Boulogeorgos, J. M. Riera and A. Alexiou, "On the joint effect of rain and beam misalignment in terahertz wireless systems," *IEEE Access*, vol. 10, pp. 58997-59012, Jun. 2022. Cited on page 2.

[6] S. Sai and L. Yang, "Performance analysis of dual-hop THz transmission systems over α-μ fading channels with pointing errors," *IEEE Internet Things J.*, vol. 9, no. 14, pp. 11772-11783, Jul. 2022. Cited 2 times on pages 2 and 7.

[7] L. Cang et al., "Terahertz MIMO communication performance analysis in exponentiated Weibull turbulence with pointing errors," *Appl. Opt.*, vol. 60, no. 24, pp. 7314-7325, Aug. 2021. Cited 2 times on pages 2 and 7.

[8] Z. Ding and H. V. Poor, "Design of THz-NOMA in the presence of beam misalignment," *IEEE Commun. Lett.*, vol. 26, no. 7, pp. 1678-1682, Jul. 2022. Cited 2 times on pages 2 and 7.

[9] O. S. Badarneh et al., "Performance analysis of FSO communications over $\mathcal{F}$ turbulence channels with pointing errors," *IEEE Commun. Lett.*, vol. 25, no. 3, pp. 926-930, Mar. 2021. Cited on page 2.

[10] V. K. Chapala, S. M. Zafaruddin, "Exact analysis of RIS-aided THz wireless systems over α-μ fading with pointing errors," *IEEE Commun. Lett.*, vol. 9, no. 14, pp. 3508-3512, Jul. 2022. Cited 2 times on pages 2 and 15.

[11] V. Palaniappan and K. Kataria, "The I-Function Distribution and Its Extensions", *Theory of Probability & Its Applications*, vol. 63, no. 2, pp. 227-245, Jan. 2018. Cited on page 2.

[12] P. Bhardwaj and S. M. Zafaruddin, "On the performance of multihop THz wireless system over mixed channel fading with shadowing and antenna misalignment," *IEEE Trans. Commun.*, vol. 70, no. 11, pp. 7748-7763, Nov. 2022. Cited on page 2.

[13] O. R. Durgada, V. K. Chapala and S. M. Zafaruddin. "RIS-THz wireless communication with random phase noise and misaligned transceiver," *ArXiv*, pp. 1-6, Nov. 2022. Cited on page 2.

[14] S. H. Alvi et al. "Performance analysis of IRS-assisted THz communication systems over α-μ fading channels with pointing errors," *Sensors*, vol. 23, no. 16, pp. 1-20, Aug. 2023. Cited on page 2.

[15] O. S. Badarneh, R. Mesleh and Y. M. Khattabi. "Reconfigurable intelligent surfaces-assisted terahertz communications," *J. Frank. Inst.*, vol. 359, no. 18, pp. 11256-11272, Dec. 2022. Cited on page 2.

[16] E. N. Papasotiriou et al., "An experimentally validated fading model for THz wireless systems," *Scientific Reports*, vol. 11, no. 18717, pp. 1-14, Sep. 2021. Cited 2 times on pages 3 and 18.

[17] E. N. Papasotiriou et al., "A new look to THz wireless links: Fading modeling and capacity assessment," in Proc. of *IEEE International Symposium on Personal, Indoor and Mobile Radio Communications*, pp. 1-5, 2021. Cited on page 3.

[18] J. Ye et al., "On outage performance of terahertz wireless communication systems," *IEEE Trans. Commun.*, vol. 70, no. 1, pp. 649-663, Jan. 2022. Cited on page 3.

[19] L. Bariah, S. Muhaidat and A. Al-Dweik, "Error probability analysis of non-orthogonal multiple access aver Nakagami-m fading channels," *IEEE Trans. Commun.*, vol. 67, no. 2, pp. 1586-1599, Feb. 2019. Cited 4 times on pages 3, 37, 38, and 40.

[20] A. M. Magableh, T. Aldalgamouni, O. Badarneh, S. Mumtaz and S. Muhaidat, "Performance of non-orthogonal multiple access (NOMA) systems over N-Nakagami-m multipath fading channels for 5G and beyond", *IEEE Trans. Veh. Technol.*, vol. 71, no. 11, Nov. 2022. Cited 2 times on pages 3 and 38.

[21] M. Li et al., "Error performance of NOMA system with outdated, imperfect CSI, and RHI over α-μ fading channels," *IEEE Trans. Veh. Technol.*, vol. 73, no. 2, pp. 2142-2155, Feb. 2024. Cited on page 3.

[22] A. Alqahtani, E. Alsusa, A. Al-Dweik and M. Al-Jarrah, "Performance analysis for downlink NOMA over α-μ generalized fading channels," *IEEE Trans. Veh. Technol.*, vol. 70, no. 7, pp. 6814-6825, Jul. 2021. Cited on page 3.

[23] Z. Ding and H. V. Poor, "Design of THz-NOMA in the presence of beam misalignment", *IEEE Commun. Lett.*, vol. 26, no. 7, pp. 1678-1682, Jul. 2022. Cited on page 3.

[24] Z. Ding and H. V. Poor, "Joint beam management and power allocation in THz-NOMA networks", *IEEE Trans. Commun.*, vol. 71, no. 4, pp. 2059-2073, Apr. 2023. Cited on page 3.

[25] J. Yuan, Z. Wang, X. Wang, B. Li, J. Lu, Y. Wang, R. Wu, Z. Wei and H. Liu, "Performance analysis of FSO/THz-RF dual-hop link based on NOMA", *Opt. Commun.*, vol. 557, Apr. 2024. Cited on page 3.

[26] H. Yahya, A. Ahmed, E. Alsusa, A. Al-Dweik and Z. Ding, "Error rate analysis of NOMA: Principles, survey and future directions" *IEEE Open J. Commun. Soc.*, vol. 4, pp. 1682-1727, Jul. 2023. Cited 2 times on pages 3 and 36.

[27] O. S. Badarneh, "Statistics of the product of two α-$\mathcal{F}$ variates with applications," *IEEE Commun. Lett.*, vol. 25, no. 6, pp. 1761-1765, Jun. 2021. Cited on page 6.

[28] Wolfram Research, Inc. (2020). *Wolfram Research*. Accessed: Aug. 21, 2024. [Online]. Available: http://functions.wolfram.com/id. Cited 6 times on pages 7, 8, 10, 11, 15, and 25.

[29] O. S. Badarneh, "The α-$\mathcal{F}$ composite fading distribution: statistical characterization and applications," *IEEE Trans. Veh. Technol.*, vol. 69, no. 8, pp. 8097-8106, Aug. 2020. Cited on page 7.

[30] R. Bhatnagar and P. Garg, "Hybrid underwater wireless system for shallow sea monitoring: An outage analysis," 2022 IEEE International Conference on Electronics, Computing and Communication Technologies (CONECCT), Bangalore, India, 2022, pp. 1-5. Cited on page 7.

[31] Q. Sun, Z. Zhang, Y. Zhang, M. López-Benítez and J. Zhang, "Performance analysis of dual-hop wireless systems over mixed FSO/RF fading channel," *IEEE Access*, vol. 9, pp. 5529-85542, 2021. Cited on page 7.

[32] Bhatnagar, R., Garg, P., "Performance analysis of hybrid underwater wireless system for shallow sea monitoring," *Photon. Netw. Commun.*, vol. 46, pp. 78–89, 2023 Cited on page 7.

[33] R. Bhatnagar and P. Garg, "Parametric evaluation of decode and forward relay based mixed wireless transmission system over α-$\mathcal{F}$ fading channels," 2023 International Conference on Sustainable Emerging Innovations in Engineering and Technology (ICSEIET), Ghaziabad, India, 2023, pp. 15-18. Cited on page 7.

[34] I. S. Ansari, F. Yilmaz and M. -S. Alouini, "Performance analysis of free-space optical links over Málaga ($\mathcal{M}$) turbulence channels with pointing errors," *IEEE Trans. Wirel. Commun.*, vol. 15, no. 1, pp. 91-102, Jan. 2016. Cited on page 7.

[35] A. A. Farid and S. Hranilovic, "Outage capacity optimization for freespace optical links with pointing errors," *J. Lightw. Technol.*, vol. 25, no. 7, pp. 1702–1710, Jul. 2007. Cited on page 7.

[36] M. T. Dabiri and M. Hasna, "Pointing error modeling of mmWave to THz high-directional antenna arrays," *IEEE Wirel. Commun. Lett.*, vol. 11, no. 11, pp. 2435-2439, Nov. 2022. Cited on page 7.

[37] I. S. Gradshteyn and I. M. Ryzhik. *Table of Integrals, Series and Products*. New York: Academic Express, 2007. Cited 9 times on pages 8, 9, 12, 14, 15, 16, 26, 27, and 39.

[38] A. P. Prudnikov, Y. A. Brychkov, and O. I. Marichev. *Integral and Series: Volume 3, More Special Functions*. Florida: CRC Press Inc., 1990. Cited on page 9.

[39] A. M. Mathai, R. K. Saxena, and H. J. Haubold. *The H-Function: Theory and Applications*. New York, NY, USA: Springer, 2009. Cited 11 times on pages 9, 10, 13, 14, 15, 16, 22, 24, 26, 28, and 39.

[40] A. A. Kilbas and M. Saigo. *H-Transforms: Theory and Applications*. Florida: CRC Press Inc, 2004. Cited 3 times on pages 10, 11, and 25.

[41] O. S. Badarneh, S. Muhaidat and D. B. da Costa, "The α-η-κ-$\mathcal{F}$ composite fading distribution", *IEEE Wirel. Commun. Lett.*, vol. 9, no. 12, pp. 2182-2186, Dec. 2020. Cited on page 10.

[42] F. Yilmaz and M. S. Alouini, "Novel asymptotic results on the high-order statistics of the channel capacity over generalized fading channels", in Proc. of *IEEE SPAWC*, pp. 389-393, Jun. 2012. Cited 2 times on pages 12 and 27.

[43] L. Wei, C. Huang, G. C. Alexandropoulos, C. Yuen, Z. Zhang, M. Debbah, "Channel estimation for RIS- empowered multi-user MISO wireless communications", *IEEE Trans. Commun.*, vol. 69, no. (6), pp. 4144–4157, 2021. Cited on page 13.

[44] Q. Wu, R. Zhang, "Towards smart and reconfigurable environment: Intelligent reflecting surface aided wireless network", *IEEE Commun. Mag.*, vol. 58, no. 1, pp. 106–112, 2020. Cited on page 13.

[45] Y. Xu, H. Chu, P. Xu, "Joint channel estimation and passive beamforming for reconfigurable intelligent surface aided multi-user massive MIMO system, in Proc. of IEEE BlackSeaCom, pp. 1-3, 2021. Cited on page 13.

[46] M. D. Springer and W. E. Thompson, "The distribution of products of independent random variables," *SIAM J. Appl. Math.*, vol. 14, no. 3, pp. 511-526, May 1966. Cited 2 times on pages 14 and 24.

[47] H. S. Silva et al., "On the sum of α-$\mathcal{F}$ and double α-$\mathcal{F}$ variates with application to MRC and RIS", *IEEE Commun. Lett.*, vol. 26, no. 12, pp. 2894-2898, Dec. 2022. Cited on page 15.

[48] J. G. Proakis and M. Salehi. *Digital Communications*. New York: McGraw-Hill, 2008. Cited on page 16.

[49] Y. A. Rahama, M. H. Ismail and M. S. Hassan, "On the sum of independent Fox's H-function variates with applications," *IEEE Trans. Veh. Technol.*, vol. 67, no. 8, pp. 6752-6760, Aug. 2018. Cited 5 times on pages 16, 26, 27, 29, and 40.

[50] A. Soulimania, M. Benjillalia, H. Chergui, D. B. da Costa, "Multihop Weibull-fading communications: performance analysis framework and applications", *J. Franklin Inst.*, vol. 358, no. 15, pp. 1-35, Aug. 2021. Cited on page 17.

[51] M. D. Yacoub. "The α-μ distribution: A physical fading model for the stacy distribution," *IEEE Trans. Veh. Technol.*, vol. 56, no. 1, pp. 27-34, 2007. Cited on page 18.

[52] Ankit Rohatgi, WebPlotDigitizer, URL: `https://automeris.io/`, version 5.2. Accessed: Oct. 03, 2024. [Online]. Cited on page 18.

[53] S. K. Yoo *et al.*, "Entropy and energy detection-based spectrum sensing over $\mathcal{F}$-composite fading channels," *IEEE Trans. Commun.*, vol. 67, no. 7, pp. 4641-4653, Jul. 2019. Cited on page 25.